State augmentation method for non-stationary/non-Gaussian vibrations of multi degree-of-freedom linear systems

Simian Lei[1, 2, 3, 4], Wei Cui[1, 2, 3, *], Liutian Zhang[1, 2, 3], Luca Patruno[4], Stefano de Miranda[4], Lin Zhao[1, 2, 3], Yaojun Ge[1, 2, 3]

[1] State Key Lab of Disaster Reduction in Civil Engineering, Tongji University, Shanghai 200092, China

[2] Department of Bridge Engineering, College of Civil Engineering, Tongji University, Shanghai 200092, China

[3] Key Laboratory of Transport Industry of Bridge Wind Resistance Technologies, Tongji University, Shanghai 200092, China

[4] DICAM, University of Bologna, Bologna, Italy

Abstract

The basic assumptions of stationary/Gaussian excitations and temporal independence in linear systems are commonly employed in stochastic dynamic analyses, facilitating various engineering investigations. However, in certain scenarios such as wind-induced vibrations under non-synoptic extreme wind, these assumptions may lead to unreliable predictions. The excitations exhibit significant non-stationary/non-Gaussian features due to the inherent non-synopticity of the flow. Moreover, when accounting for motion-induced forces, the coupled aerodynamic-mechanical system is modeled as a linear time-varying system marked by time-dependent aerodynamic damping and stiffness. This study aims to introduce a state augmentation method for examining the multi-modal vibrations of a long-span bridge excited by non-synoptic winds. Both unsteady motion-induced forces and non-stationary/non-Gaussian turbulence-induced forces are considered to predict the buffeting response. Based on stochastic calculus theory and the stars and bars method, we derive equations governing the statistical moments of all orders for the response of a dynamic system with multiple degrees of freedom. A comprehensive buffeting analysis of the model bridge to all wind segments of Typhoon Hagupit is conducted by using the proposed method, showing potentially greater responses when considering the non-synoptic features of the wind.

Keywords

Non-synoptic wind; Multi-modal buffeting; State augmentation method; Linear time-varying system; Stochastic differential equation.

1 Introduction

The analysis of dynamic systems under stochastic excitations has gained significance within mechanical and structural engineering in recent decades (Benfratello and Muscolino, 1999), stemming from an increased awareness of the necessity to evaluate the reliability of structures through a

* Corresponding author, E-mail address: cuiwei@tongji.edu.cn (W. Cui).

This is the accepted manuscript version of the article.
The final published version of this article is available at https://doi.org/10.1016/j.jweia.2024.105747

probabilistic point of view. In many scenarios, the characteristics of the structural system and the excitation are assumed to be independent of time. Excitations are often regarded as stationary/Gaussian processes, and systems are assumed to be linear time-invariant. These assumptions generally yield satisfactory accuracy across a wide spectrum of applications, such as the case of train-track coupled systems subjected to stochastic irregularities (Lei et al, 2022b) and synoptic wind effects (Davenport, 1967; Isyumov, 2012) on civil structures including buildings and bridges. Nonetheless, there are instances where these hypotheses might falter, resulting in inaccuracies. For instance, the condition of the train traversing the bridge introduces time-varying characteristics to the coupled system (Lombaert and Conte, 2012). Similarly, extreme wind phenomena such as hurricanes and thunderstorms often exhibit notable non-synoptic features (Huang et al, 2015; Zhao et al, 2019), having time-varying means and high turbulence intensity. The introduction of non-stationary/non-Gaussian excitations and time-dependent characteristics of the system poses significant challenges to stochastic dynamic analysis.

In this paper the emphasis lies on structural vibrations induced by extreme non-synoptic winds, a topic that has garnered significant attention in recent years (Huang et al, 2015; Zhao et al, 2019). In these scenarios, rapid changes in non-synoptic airflow have the potential to amplify aerodynamic forces, leading to increased responses (Kareem, 2009). When taking account of aeroelastic effects (Brusco and Solari, 2021), the wind-structure coupled system is represented as a linear time-varying (LTV) system (Hu et al, 2013), accounting for the time-varying mean wind speeds that render the aerodynamic damping and stiffness time-dependent. It is crucial to acknowledge that for LTV systems (Zadeh, 1950) the system response will be not stationary even if the excitations are assumed as stationary. Brusco and Solari (Brusco and Solari, 2021) considered the aeroelastic forces by invoking quasi-steady theory and computed the dynamic responses of slender structures subjected to thunderstorm outflows, employing time-domain integration of motion equations. Nevertheless, the literature regarding those effects remain limited, as classical methodologies mainly aim at synoptic wind conditions (Kareem et al, 2019). Consequently, it proves cumbersome to evaluate the statistics of the non-stationary/non-Gaussian responses (Davenport, 1967; Isyumov, 2012), especially when considering unsteady aerodynamic effects.

Certainly, Monte Carlo simulations can address these concerns (Huang et al, 2013), by employing multiple deterministic time-history samples derived from the evolutionary power spectral density (Priestley, 1967; Priestley, 1965) to statistically characterise the non-stationary response. However, they lack the capability to offer physical insights into the problem (Denoël and Carassale, 2015), and become computationally intensive when employing sufficiently numerous samples for reliable results (Benfratello and Muscolino, 1999). Inspired by Davenport's seminal work (Davenport, 1967; Isyumov, 2012) and Priestley's Evolutionary Spectra theory (Priestley, 1967; Priestley, 1965), Kareem et al. (Kareem et al, 2019) extended the well-known wind loading chain, initially employed for stationary buffeting analysis in the frequency-domain, to encompass a non-stationary regime in the time-frequency domain. Within this framework, the response spectrum is determined as the product (Chen,

2008) of the time-frequency wind spectrum, the instantaneous aerodynamic admittance, and the structural transfer function. Subsequently, this framework was applied (Chen, 2015) to predict non-stationary buffeting responses involving motion-induced forces. To address the system with time-dependent characteristics, the generalized frequency-domain method treats the system as time-invariant within a moving short window (Guo and Kareem, 2016; Tao et al, 2020). This simplifies the task to identifying the time-independent transfer function and stationary responses of the equivalent invariant system within each window. Note that this methodology is only viable for systems exhibiting slowly time-varying characteristics. Lin et al. (Lin et al, 1994) proposed an alternative time-frequency approach, i.e., pseudo excitation method, offering the advantage of simultaneously addressing non-stationary excitations and time-varying systems (Hu et al, 2017; Tao et al, 2020). This method expands pseudo excitations in the frequency domain and subsequently integrates pseudo responses in the time domain. Despite its versatility, its computational time, as highlighted in (Lu et al, 2009), is predominantly consumed during the integration process and is roughly proportional to the number of frequencies. This aspect raises concerns for time-frequency techniques, particularly when interest lies only in the statistical moments of responses rather than the spectrum. Though the Precise Integration Method (Zhang et al, 2010) can improve the efficiency, it still involves a detour in the frequency domain.

Alongside the aforementioned contributions, a foundational investigation addressing this issue was introduced by Grigoriu (Grigoriu, 2013; Grigoriu and Ariaratnam, 1988; Grigoriu and Field Jr, 2014). This study employed stochastic calculus (Karlin and Taylor, 1981) and Itô's formula (Itô, 1944) to investigate a linear system subjected to stationary non-Gaussian excitations represented as polynomials of Gaussian processes with time-dependent coefficients. The concept of this method lies in the potential approximation of excitations through filtered Brownian motions (Benfratello and Muscolino, 1999). This allows the transformation of dynamic equations into stochastic differential equations. Then, by means of Itô's formula, the statistical moments of the responses are directly evaluated by solving the termed statistical moment equations with high efficiency and without detouring in the frequency domain. Subsequently, several researchers extensively explored the potential of this method, not only for non-Gaussian excitations (Benfratello et al, 1996; Benfratello and Muscolino, 1999; Gullo et al, 1998) but also for nonlinear systems with parametric and nonlinear excitations (Sun and Hsu, 1987; Wojtkiewicz et al, 1996). In instances of non-Gaussian scenarios, larger dimension statistical moment equations could be derived, forming a closed system of algebraic equations, allowing for the accurate computation of higher-order statistical moments to characterize the non-Gaussian features of responses. Recently Cui et al. (Cui et al, 2022) revisited this concept and computed the statistical moments of buffeting responses of a long-span bridge subjected to stationary non-Gaussian turbulence, factoring in the multi-modal coupling effect. In the latter case, when dealing with nonlinearity, which renders the system unclosed, additional closure techniques such as the cumulant-neglect closure method (Soong and Grigoriu, 1993) need to be introduced to enable moment

equations solvable.

As reviewed above, the moment equation method has been applied in various stochastic dynamic problems. However, its application for non-stationary analysis, particularly involving time-dependent system characteristics, remains rare. A recent study by Lei et al. (Lei et al, 2022a) showcased the method's potential in non-stationary buffeting analysis factoring in motion-induced forces, which alters the methodology substantially, transitioning from algebraic equations in stationary cases to differential equations in non-stationary scenarios. Nevertheless, this application was confined to a single degree-of-freedom system, employing the quasi-steady assumption (Brusco and Solari, 2021) to model aerodynamic forces. Given the important role of unsteady aerodynamic effects in buffeting analysis for long-span bridges (Barni et al, 2021; Barni et al, 2022; Jain et al, 1996), accurate modeling of motion-induced and turbulence-induced forces becomes crucial. Additionally, addressing multi-modal vibrations, as suggested by Cui [34], complicates the derivation of statistical moment equations. Therefore, to widen the applicability of the moment equation method, it is imperative to resolve issues arising from unsteady aerodynamic forces and multi-modal vibrations.

This study intends to introduce a state augmentation method to conduct a comprehensive analysis of multi-modal vibrations of a long-span bridge subjected to non-synoptic winds. The analysis includes accounting for unsteady motion-induced forces and non-stationary/non-Gaussian turbulence-induced forces to predict the buffeting responses. Considering the time-dependent aerodynamic damping and stiffness, the equation of motion of the wind-structure coupled system is expressed as an LTV system. By performing the defined $\mathcal{M}$ transform of the corresponding Fokker–Planck equation, the statistical moments of the responses are obtained through solving a first-order ordinary differential equation system. The proposed method is firstly applied to calculate the buffeting responses to two selected 10-min wind segments in detail, as an illustration of the non-stationary feature and non-Gaussian feature of buffeting responses induced by non-synoptic winds. A thorough buffeting analysis of the model bridge to all wind segments of Typhoon Hagupit is subsequently conducted. This study is considered as a follow-up to previous research by the authors (Lei et al, 2022a) in order to extend the previous single degree-of-freedom investigation to a multi degree-of-freedom case and incorporate the unsteady aerodynamic effect.

2 Non-synoptic features of typhoon

Recent advancements in high-frequency wind field monitoring devices including ultrasonic anemometer have provided deeper insights into the characteristics of turbulence in the atmospheric boundary layer. Extreme winds such as typhoons always present obvious non-synoptic characteristics, featuring non-stationary wind speed and high turbulence intensity. Intriguingly, these non-synoptic features rarely coincide due to their different formation mechanisms. The non-stationary characteristic appears during the passage of the typhoon eye, encircled by the eyewall where the highest wind speeds are found, resulting in great variations in both wind direction and wind speed trend. Notice that substantial variations in wind trends may exaggerate the variance of wind fluctuations, partly due to a

mixture of large-amplitude low-frequency components when the stationary assumption is applied. By filtering out the varying wind speed trend, the variance of resultant wind fluctuations decreases, thereby leading to a reduced turbulence intensity. In contrast, high turbulence intensity often occurs within a relatively low range of mean wind speeds, typically between 10 and 20 $\mathrm{m/s}$, where the wind speed trend tends to be stationary, rendering it unlikely to lower the turbulence intensity by removing the low-frequency trend. In this context, these non-synoptic effects on buffeting analysis will be considered independently in Section 4.3.

In September 2008, Typhoon 'Hagupit' (No. 200814), forming in western Pacific Ocean on 15th September, strengthened into a strong typhoon on 22nd September and moved to South China Sea on 23rd September, with the highest wind speed at about 50 m/s close to its centre and the lowest air pressure 935 hPa. A 24-hour wind speeds in three axes were recorded by the anemometer from 23rd September at 18:00 (GMT+8) until 24th September at 18:00 (GMT+8) during Typhoon 'Hagupit'. The high-precision 3-axis ultrasonic anemometer was located at an elevation of 60 m on an observation tower (111.38°E, 21.45°N), and the wind data was sampled at 10 Hz. Detailed information on the measurement campaign can be found in (Liu et al, 2021; Zhang et al, 2023). The acquired wind speed data was decomposed as mean wind speeds and three orthogonal wind fluctuation components. The longitudinal wind is assumed to be orthogonal to the bridge axis in the buffeting analysis and the vertical turbulence is regarded as zero-mean process. Fig. 1 displays time histories of the decomposed longitudinal wind speeds recorded during Typhoon Hagupit passing over China on 23-24th September 2008. The data on vertical turbulence is given in Appendix A. The wind speed histories feature an 'M' shape which is typical of Typhoon processes due to its eye passage.

To illustrate its non-synoptic natures, the wind record is subdivided into 10-minute time series, giving a total of 144 segments. Fig. 2 shows the 10-minute averaged wind speed $\overline{U}_{10}$ (red solid line with triangle markers) and the corresponding longitudinal turbulence intensity $I_{u,10}$ (cyan dashed line with circle markers) of each segment when treated as stationary. The corresponding statistic on vertical turbulence is given in Appendix A. It is found that, apart from Segment No. 61, turbulence intensities exceeding 15% are consistently associated with low mean wind speeds. The high turbulence intensity of Segment No. 61 mainly arises from its significantly varying wind speed trend, i.e., the non-stationary nature, as will be demonstrated in the following.

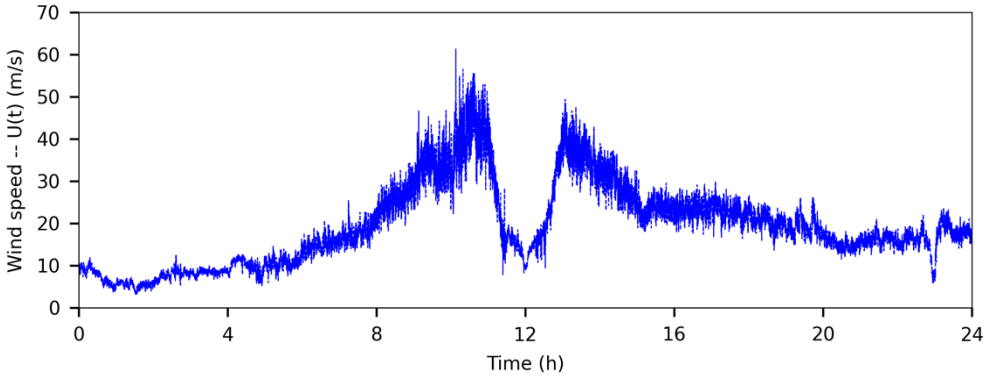

Fig. 1. Time history of longitudinal wind speeds of Typhoon Hagupit recorded in September 2008.

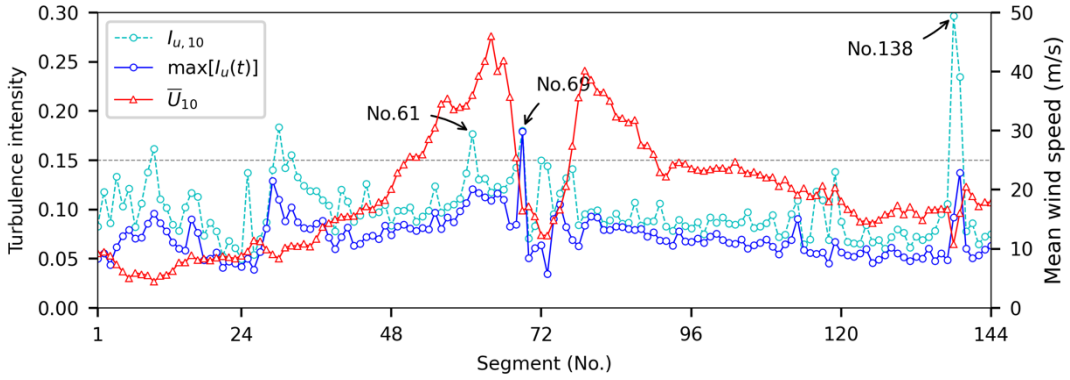

Fig. 2. Mean wind speeds and longitudinal turbulence intensities of the subdivided 10-minture segments of Typhoon Hagupit.

Non-stationary wind speed $U(t)$ can be characterized as the sum of a deterministic time-varying mean $\overline{U}(t)$ and a zero-mean non-stationary fluctuating component $u(t)$. Due to the slower variation of $\overline{U}(t)$ compared to $u(t)$, the structure tends to react statically when subjected to time-varying mean wind, allowing for the employment of the quasi-static method. The time-varying mean and zero-mean non-stationary fluctuation are extracted by employing the discrete wavelet transform, with the 20th order Daubechies wavelet as the analyzing wavelet and an 8-level decomposition of the signal. Notice that due to the existence of time-dependent mean wind speeds, the turbulence intensity also varies over time, necessitating a revised definition, e.g., $I_u(t) = \sigma_u(t)/\overline{U}(t)$ as proposed in (Huang et al, 2015). The maximal modified time-varying turbulence intensity for each segment is depicted as the blue solid line with circle markers in Fig. 2. Remarkably, the incorporation of non-stationary features has noticeably reduced turbulence intensities, particularly Segments No. 61 and No. 138. To illustrate the non-stationary feature, Fig. 3 (a) and (b) show the time-varying means and zero-mean longitudinal fluctuations of Segments No. 61 and No. 138, respectively, and the vertical turbulence counterparts are given in Appendix A. In Fig. 3, significant variations in mean wind speeds are observed in both segments, and upon removal of the time-varying mean the turbulence intensities decrease substantially.

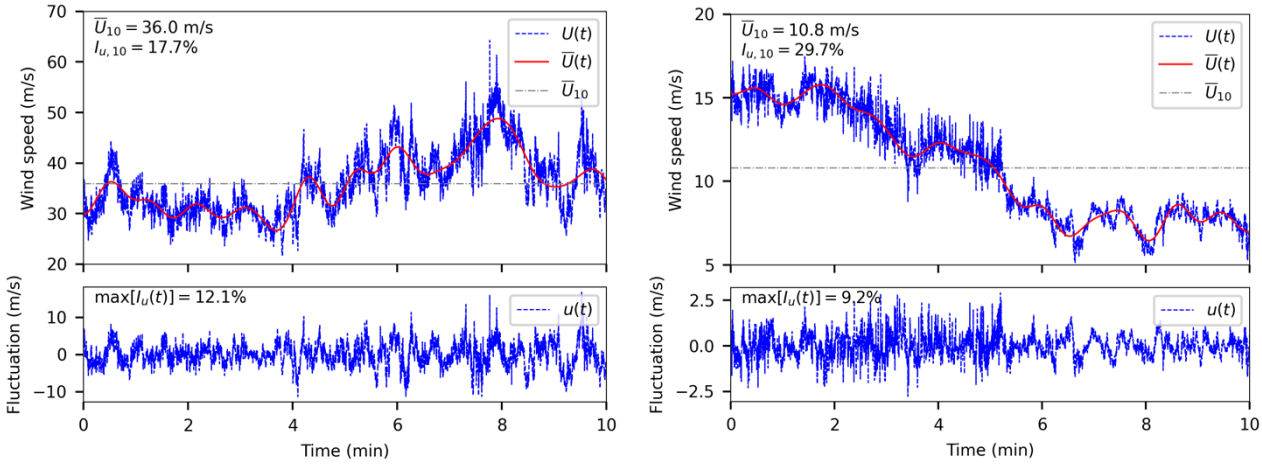

(a) Segment No. 61 (b) Segment No. 138

Fig. 3. Wind speed model extracted from the selected longitudinal wind segments from Typhoon Hagupit record.

Under high turbulence intensity, the consequent buffeting forces exhibit obvious non-Gaussian feature due to the notable contribution of quadratic terms of turbulence in wind pressure, resulting in potentially amplified extreme responses. Studies (Kareem et al, 1998; Zhang et al, 2023) indicate that a 15% turbulence intensity may cause a 10% increase in buffeting force RMS and a 25% increase in the peak factor compared to the Gaussian results. This effect intensifies further when the nonlinearity of aerodynamic coefficients is included (Denoël and Degée, 2006), resulting in more pronounced non-Gaussian features marked by higher skewness and kurtosis. For instance, Fig. 4 displays the time history of strong longitudinal turbulence of Segment No. 69, with a turbulence intensity of 18%. The time history of vertical turbulence is given in Appendix A. The segment exhibits subtle non-stationary characteristic, and the removal of the mean wind trend does not substantially mitigate the turbulence intensity. To illustrate non-Gaussian features of buffeting forces, the non-Gaussian drag force is calculated by including the quadratic terms and nonlinear aerodynamic coefficients in a quasi-steady manner, which can be referred to (Denoël and Degée, 2006) and will be shown later by Eq. (29) in Section 4. The computation considers the parameters listed in Table 2 in Section 5. Table 1 reports the statistics of the turbulence and the induced non-Gaussian drag force and Gaussian counterpart per unit length. The skewness is computed as the Fisher-Pearson standardized coefficient of the third-order statistical moment. The results indicate a 6% rise in the mean value and 8% rise in the standard deviation of the non-Gaussian force along with greater skewness in contrast to the Gaussian one.

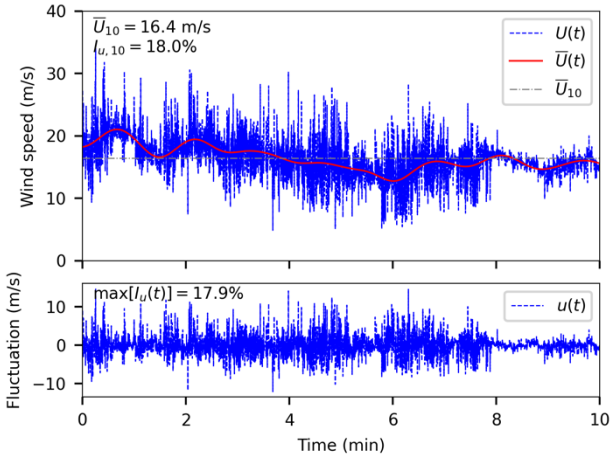

Fig. 4. Strong longitudinal turbulence of Segment No. 69 from Typhoon Hagupit record.

Table 1. Statistics of the turbulence and the Gaussian and non-Gaussian drag forces per unit length.

Data	Mean	Std	Skewness
Wind speed	16.4 m/s	2.96 m/s	0.24
Gaussian force	6.93 kN/m	2.42 kN/m	0.27
Non-gaussian force	7.33 kN/m	2.61 kN/m	1.88

3 Formulation of state augmentation method

3.1 Statement of the problem

Suppose a linear time-varying (LTV) system with N degree-of-freedom (MDOF) subjected to non-stationary non-Gaussian excitations. The equation of motion is described by a set of linear ordinary differential equations with coefficients varying with time

$$\mathbf{M}\ddot{\mathbf{X}} + \mathbf{C}(t)\dot{\mathbf{X}} + \mathbf{K}(t)\mathbf{X} = \mathbf{F}(t) \tag{1}$$

in which $\mathbf{M}$, $\mathbf{C}(t)$ and $\mathbf{K}(t)$ are matrices of mass, damping and stiffness, respectively. $\mathbf{C}(t)$ and $\mathbf{K}(t)$ are the known time-varying coefficients. $\mathbf{X}$ is the displacement response, and $\mathbf{F}(t)$ is the non-stationary non-Gaussian excitation.

Unlike the stationary process that has a specific definition of power spectrum, the non-stationary process can be defined in various ways (Huang et al, 1998; Page, 1952; Wickerhauser, 1992). This study is restricted only to the evolutionary process established by Priestley (Priestley, 1967; Priestley, 1965), the one from which the evolutionary spectrum can be derived. This non-stationary process holds more physical sense in terms of energy distribution and could be regarded as the output of a time-variable filter with a stationary process passing through. For the sake of simplicity, a uniformly modulated polynomial model (Huang et al, 2015) is adopted to represent the evolutionary non-Gaussian excitation $\mathbf{F}(t)$

$$\mathbf{F}(t) = \sum_{i=1}^{l} \mathbf{A}_i(t)\mathrm{diag}(\mathbf{F}_s)^{i-1}\mathbf{F}_s \tag{2}$$

in which $\mathbf{A}(t)$ is the diagonal matrix of time-modulation functions, and $\mathbf{F}_s(t)$ is the corresponding

stationary Gaussian process. l is the degree of the polynomial of $\mathbf{F}_s$. Notice that, as a methodology presentation, Eq. (2) represents a general situation where excitations exhibit non-stationary and non-Gaussian features simultaneously. Considering the practical typhoon event, e.g., Typhoon Hagupit, where the non-synoptic features rarely coincide, the unified model can seamlessly adapt to two different problems considered in the follow-up analysis. Particularly, Eq. (2) will be non-stationary Gaussian forces if $l = 1$, and be stationary non-Gaussian forces if $\mathbf{A}_i$ is time-invariant. They are applicable to most practical engineering problems (Huang et al, 2013).

By substituting Eq. (2) into Eq. (1), the equation of motion is transformed to its state-space form

$$\mathrm{d}\begin{bmatrix}\mathbf{X}\\ \dot{\mathbf{X}}\end{bmatrix} = \begin{bmatrix}\mathbf{0} & \mathbf{I}\\ -\mathbf{M}^{-1}\mathbf{K}(t) & -\mathbf{M}^{-1}\mathbf{C}(t)\end{bmatrix}\begin{bmatrix}\mathbf{X}\\ \dot{\mathbf{X}}\end{bmatrix}\mathrm{d}t + \begin{bmatrix}\mathbf{0}\\ \mathbf{M}^{-1}\sum_{i=1}^{l}\mathbf{A}_i(t)\mathrm{diag}(\mathbf{F}_s)^{i-1}\mathbf{F}_s\end{bmatrix}\mathrm{d}t \tag{3}$$

3.2 Augmented states of the system and the excitation

According to (Grigoriu, 2013; Grigoriu and Ariaratnam, 1988), the stationary Gaussian process $\mathbf{F}_s(t)$ can be approximated by a multivariate Ornstein-Uhlenbeck (OU) process, denoted as $\mathbf{Z}(t)$. As a general methodology presentation, $\mathbf{Z}(t)$ is considered to be of size M, which includes the situation where the number of OU processes required for loading may exceed the number of degrees of freedom in the structure or the concerned natural modes, i.e., N, as will be shown in the non-stationary case in Section 4. In this current section, $M = N$. $\mathbf{Z}(t)$ satisfies the stochastic differential equation

$$\mathrm{d}\mathbf{Z}(t) = -\boldsymbol{\alpha}\mathbf{Z}(t)\mathrm{d}t + \boldsymbol{\Theta}\mathrm{d}\mathbf{W}(t) \tag{4}$$

in which $\boldsymbol{\alpha}$ and $\boldsymbol{\Theta}$ are positive definite matrices and not necessarily symmetric. $\mathbf{W}(t)$ is a multivariate standard Wiener process with M mutually independent components and satisfies $\mathrm{E}[\mathrm{d}\mathbf{W}\cdot\mathrm{d}\mathbf{W}^{\mathrm{T}}] = \mathbf{I}\mathrm{d}t$ where $\mathrm{E}[\cdot]$ indicates the expectation operator and $\mathbf{I}$ is the identity matrix of size M. The matrices $\boldsymbol{\alpha}$ and $\boldsymbol{\Theta}$ can be determined by fitting the autocorrelation matrix $\mathbf{R}_{\mathbf{ZZ}}(\tau) = \mathrm{e}^{-\boldsymbol{\alpha}|\tau|}\mathrm{K}_{\mathbf{ZZ}}$ or the double-side power spectral density matrix $\mathbf{S}_{\mathbf{ZZ}}(\mathrm{j}\omega) = (-\mathrm{j}\omega\mathbf{I}+\boldsymbol{\alpha})^{-1}\boldsymbol{\Theta}\boldsymbol{\Theta}^{\mathrm{T}}(\mathrm{j}\omega\mathbf{I}+\boldsymbol{\alpha}^{\mathrm{T}})^{-1}$ with the ones of $\mathbf{F}_s(t)$, in which $\mathbf{K}_{\mathbf{ZZ}}$ is the auto-covariance matrix of $\mathbf{Z}$ and can be determined from the Lyapunov equation (Lyapunov, 1892)

$$\boldsymbol{\alpha}\mathbf{K}_{\mathbf{ZZ}} + \mathbf{K}_{\mathbf{ZZ}}\boldsymbol{\alpha}^{\mathrm{T}} = \boldsymbol{\Theta}\boldsymbol{\Theta}^{\mathrm{T}} \tag{5}$$

The fitting procedure will be shown in Section 5.

By substituting Eq. (4) into Eq. (3), the augmented states of the system and the excitation are assembled as

$$\mathrm{d}\begin{bmatrix}\mathbf{X}\\ \dot{\mathbf{X}}\\ \mathbf{Z}\end{bmatrix} = \begin{bmatrix}\mathbf{0} & \mathbf{I} & \mathbf{0}\\ -\mathbf{M}^{-1}\mathbf{K}(t) & -\mathbf{M}^{-1}\mathbf{C}(t) & \mathbf{M}^{-1}\sum_{i=1}^{l}\mathbf{A}_i(t)\mathrm{diag}(\mathbf{Z})^{i-1}\\ \mathbf{0} & \mathbf{0} & -\boldsymbol{\alpha}\end{bmatrix}\begin{bmatrix}\mathbf{X}\\ \dot{\mathbf{X}}\\ \mathbf{Z}\end{bmatrix}\mathrm{d}t + \begin{bmatrix}\mathbf{0}\\ \mathbf{0}\\ \boldsymbol{\Theta}\end{bmatrix}\mathrm{d}\mathbf{W} \tag{6}$$

Eq. (6) is usually recognized as an Itô-type stochastic differential equation (Karlin and Taylor, 1981) of the form

$$\mathrm{d}\mathbf{Y} = \mathbf{g}(\mathbf{Y},t)\mathrm{d}t + \mathbf{h}(\mathbf{Y},t)\mathrm{d}\mathbf{W} \tag{7}$$

in which $\mathbf{Y}$ is the augmented state vector of size $2N+M$. $\mathbf{g}(\mathbf{Y},t)$ and $\mathbf{h}(\mathbf{Y},t)$ are explicit functions of the states $\mathbf{Y}$ and time t, of which the expressions are given in Appendix B.

3.3 Equations of statistical moments

According to statistical mechanics and information theory, the time evolution of the probability density function $p(\mathbf{Y},t)$ of the augment states $\mathbf{Y}$ described by the stochastic differential equation Eq. (7) satisfies the Fokker–Planck equation

$$\frac{\partial}{\partial t}p(\mathbf{Y},t) = -\sum_{i=1}^{2N+M}\frac{\partial}{\partial Y_i}[g_i(\mathbf{Y},t)p(\mathbf{Y},t)] + \frac{1}{2}\sum_{i=1}^{2N+M}\sum_{j=1}^{2N+M}\frac{\partial^2}{\partial Y_i \partial Y_j}\left[(\mathbf{h}\mathbf{h}^{\mathrm{T}})_{ij}p(\mathbf{Y},t)\right] \tag{8}$$

in which Y_i is the i-th element of the augmented state $\mathbf{Y}$, and g_i is the i-th element of the vector $\mathbf{g}(\mathbf{Y},t)$.

Assume $\xi(\mathbf{Y})$ as the product function of the augmented states $\mathbf{Y}$

$$\xi(\mathbf{Y}) = \prod_i^N X_i^{a_i}\prod_i^N \dot{X}_i^{b_i}\prod_i^M Z_i^{f_i} \tag{9}$$

in which X_i, $\dot{X}_i$ and Z_i are the i-th element of the states $\mathbf{X}$, $\dot{\mathbf{X}}$ and $\mathbf{Z}$, respectively. The superscripts a_i, b_i and f_i are the corresponding exponents which are non-negative integers. The $\mathcal{M}$ transform of a scalar function $f(\mathbf{Y},t)$ is then defined as the form

$$\mathcal{M}\{f\}(a_1,\cdots,a_N,b_1,\cdots,b_N,f_1,\cdots,f_M) = \int_{-\infty}^{\infty}\cdots\int_{-\infty}^{\infty} f(\mathbf{Y},t)\xi(\mathbf{Y})\mathrm{d}Y_1\cdots\mathrm{d}Y_{2N+M} \tag{10}$$

Obviously, the $\mathcal{M}$ transform of the probability density function $p(\mathbf{Y},t)$ is the statistical moment of the augmented states $\mathbf{Y}$, i.e., $\mathcal{M}\{p\} = \mathrm{E}\left(\prod_i^N X_i^{a_i}\prod_i^N \dot{X}_i^{b_i}\prod_i^M Z_i^{f_i}\right)$.

By taking the $\mathcal{M}$ transform of both sides of Eq. (8), one can obtain

$$\frac{\mathrm{d}}{\mathrm{d}t}\mathrm{E}[\xi] = \sum_i^{2N+M}\mathrm{E}\left[\frac{\partial \xi}{\partial Y_i}g_i\right] + \frac{1}{2}\sum_i^{2N+M}\sum_j^{2N+M}\mathrm{E}\left[(\mathbf{h}\mathbf{h}^{\mathrm{T}})_{ij}\frac{\partial^2\xi}{\partial Y_j\partial Y_i}\right] \tag{11}$$

In particular, $\mathrm{dE}[\xi]/\mathrm{d}t$ is not zero if $\mathbf{Y}$ is a non-stationary process (Grigoriu and Ariaratnam, 1988). The detailed derivation of Eq. (11) is given in Appendix C.

By substituting Eq. (9) into Eq. (11), Eq. (11) is expanded as

$$\begin{aligned}\frac{\mathrm{d}}{\mathrm{d}t}\mathrm{E}\left[\prod_i^N X_i^{a_i}\prod_i^N \dot{X}_i^{b_i}\prod_i^M Z_i^{f_i}\right] &= \sum_{r=1}^N a_r\mathrm{E}\left[X_r^{-1}g_r\prod_i^N X_i^{a_i}\prod_i^N \dot{X}_i^{b_i}\prod_i^M Z_i^{f_i}\right]\\ +\sum_{r=1}^N b_r\mathrm{E}\left[\dot{X}_r^{-1}g_{r+N}\prod_i^N X_i^{a_i}\prod_i^N \dot{X}_i^{b_i}\prod_i^M Z_i^{f_i}\right] &+ \sum_{r=1}^M f_r\mathrm{E}\left[Z_r^{-1}g_{r+2N}\prod_i^N X_i^{a_i}\prod_i^N \dot{X}_i^{b_i}\prod_i^M Z_i^{f_i}\right]\\ &+\frac{1}{2}\sum_{\substack{r=1\\ r\neq s}}^M\sum_{s=1}^M(\mathbf{\Theta}\mathbf{\Theta}^{\mathrm{T}})_{rs}f_rf_s\mathrm{E}\left[Z_r^{-1}Z_s^{-1}\prod_i^N X_i^{a_i}\prod_i^N \dot{X}_i^{b_i}\prod_i^M Z_i^{f_i}\right]\\ &+\frac{1}{2}\sum_{r=1}^M(\mathbf{\Theta}\mathbf{\Theta}^{\mathrm{T}})_{rr}f_r(f_r-1)\mathrm{E}\left[Z_r^{-2}\prod_i^N X_i^{a_i}\prod_i^N \dot{X}_i^{b_i}\prod_i^M Z_i^{f_i}\right]\end{aligned} \tag{12}$$

Denote the statistical moment as $\mathrm{m}(a_1,\cdots,a_N,b_1,\cdots,b_N,f_1,\cdots,f_M)$ and the summations $s=\sum_{i=1}^{N}(a_i+b_i)$ and $s_f=\sum_{i=1}^{M}f_i$ as the moment order, and so $\mathrm{m}(a_1,\cdots,a_N,b_1,\cdots,b_N,f_1,\cdots,f_M)$ is furtherly denoted as $\mathrm{m}(s,s_f)$ for the sake of brevity. By this means, the left-hand side of Eq. (12) is denoted as $\dot{\mathrm{m}}(s,s_f)$, representing the first derivative of the moment in s-th and s_f-th order. In the right-hand side, the first three summations consist of the first-order partial derivative and the function $\mathbf{g}$. Notice that $\mathbf{g}$ is the linear combination of $\mathbf{X}$, $\dot{\mathbf{X}}$ and $\mathbf{Z}^i$ in the order i from 1 to l. This gives rise to the moments $\mathrm{m}(s,s_f)$ in the order of s and s_f, and the moments $\mathrm{m}(s-1,s_f+i)$ in the order of $s-1$ and s_f+i with $i=1,2,\cdots,l$, in a different combination of exponents. The last two summations of Eq. (12) consist of the second-order partial derivative and the constant matrix $\mathbf{h}$, giving the corresponding moments $\mathrm{m}(s,s_f-2)$ in the order of s and s_f-2. In particular, the moments are zero if any exponent takes on negative values, and $\mathrm{m}(s=0,s_f)$ is the known statistical moments of OU processes in the case of $a_i=b_i=0$.

For a prescribed order of s and s_f, substituting all the combinations of the exponents into Eq. (12) gives

$$\dot{\mathbf{m}}(s,s_f)=\mathbf{P}_1(t)\mathbf{m}(s,s_f)+\mathbf{P}_2(t)\mathbf{m}(s,s_f-2)+\mathbf{Q}_1(t)\mathbf{m}(s-1,s_f+1)+\cdots+\mathbf{Q}_l(t)\mathbf{m}(s-1,s_f+l) \quad (13)$$

in which $\mathbf{m}(s,s_f)$ and $\mathbf{m}(s,s_f-2)$ are the vectors of all the unknown statistical moments in the order of s,s_f and s,s_f-2, respectively. $\mathbf{P}_1$, $\mathbf{P}_2$ and $\mathbf{Q}_1$ to $\mathbf{Q}_l$ are the known coefficient matrices.

Notice that to calculate the moments $\mathbf{m}(s,s_f)$ in the current order s,s_f requires the moments in a previous order $s-1$ and s_f+i with $i=1,2,\cdots,l$ to be determined. This leads to an explicit recursive process which is closed by imposing the boundary condition of the known $\mathbf{m}(s=0,s_f)$. Therefore, to determine the moments $\mathbf{m}(s,s_f=0)$ in the order of s and $s_f=0$, it is possible to assemble all the dependent moments into a single equation

$$\frac{\mathrm{d}}{\mathrm{d}t}\begin{bmatrix}\mathbf{m}(s,0)\\ \mathbf{m}(s-1,0)\\ \vdots\\ \mathbf{m}(s-1,l)\\ \vdots\\ \mathbf{m}(1,0)\\ \vdots\\ \mathbf{m}(1,(s-1)l)\end{bmatrix}=\mathbf{P}(t)\begin{bmatrix}\mathbf{m}(s,0)\\ \mathbf{m}(s-1,0)\\ \vdots\\ \mathbf{m}(s-1,l)\\ \vdots\\ \mathbf{m}(1,0)\\ \vdots\\ \mathbf{m}(1,(s-1)l)\end{bmatrix}+\mathbf{Q}(t)\begin{bmatrix}\mathbf{m}(0,sl)\\ \vdots\\ \mathbf{m}(0,1)\end{bmatrix} \quad (14)$$

The above formulas are the basis of the state augmentation method (SAM). It is seen that the

statistical moments satisfy a first-order ordinary differential equation system reported in Eq. (14), and for each order s, the moments can be directly obtained by solving it with prescribed initial conditions, without going through an intermediate step, e.g., the response spectra.

3.4 Exponent combinations

Prior to assembling the differential equations given in Eq. (14), it is necessary to determine the exponent combinations of the statistical moments in a requisite order, e.g., s and $s_f = 0$, in other words, to determine all the possible solutions to a single linear equation with multiple variables

$$a_1 + \cdots + a_N + b_1 + \cdots + b_N = s \tag{15}$$

required that all the variables are non-negative integers, i.e., $a_i \geq 0$ and $b_i \geq 0$, which is equivalent to the equation

$$a_1' + \cdots + a_N' + b_1' + \cdots + b_N' = s + 2N \tag{16}$$

with the converted variables $a_i' = a_i + 1 \geq 1$ and $b_i' = b_i + 1 \geq 1$.

By this means, the problem can be solved by using the stars and bars method (Feller, 1991) from combinatorics. Suppose $s + 2N$ undistinguished stars to be placed into $2N$ distinguished bins, and no bin is allowed to be empty. This can be achieved by placing $2N - 1$ bars between the stars with at most one bar in each gap and then assigning piles of stars to bins in sequence, as shown in Fig. 5.

★★★★|★|★★|★★★★★|★

Fig. 5. $2N - 1$ bars give rise to $2N$ bins containing a total of $s + 2N$ stars.

The number of all the combinations is $\mathrm{C}_{s+2N-1}^{2N-1}$, meaning $2N - 1$ from $s + 2N - 1$ gaps are chosen to contain each bar. An example of how the stars and bars method is implemented is elaborated in Appendix D. By combing this method with symbolic calculations (Meurer et al, 2017), the moment equations for any order of the statistical moments of the responses and for the dynamic system with an arbitrary number of degrees of freedom can be automatically assembled.

4 Non-stationary/non-Gaussian buffeting of long-span bridges

4.1 Equations of deck motions

The proposed state augmentation method is applied to calculate the stochastic vibrations of the bridge deck of a long-span bridge subjected to non-synoptic winds. In this study, the wind speeds are assumed to be orthogonal to the bridge longitudinal axis, as mentioned in Section 2. Therefore, the effect of skew winds (da Costa et al, 2022) is disregarded. Flexible structures such as long-span bridges always possess closely spaced modal frequencies (Jain et al, 1996). When considering motion-induced forces, the consequent aerodynamic damping and stiffness may potentially affect the structure dynamic properties and thus lead to considerable coupling effect in multi-modal vibrations. Therefore, the self-excited forces and the non-stationary/non-Gaussian turbulence-induced forces, i.e., buffeting forces, are included both to predict the buffeting responses.

The equation of motion of the bridge deck subjected to aerodynamic forces is expressed as

$$\mathbf{M}_d\ddot{\mathbf{X}}_d + \mathbf{C}_d\dot{\mathbf{X}}_d + \mathbf{K}_d\mathbf{X}_d = \mathbf{F}^{se} + \mathbf{F}^{b} \tag{17}$$

in which $\mathbf{M}_d$, $\mathbf{C}_d$ and $\mathbf{K}_d$ are the mass, damping and stiffness matrices, respectively. $\mathbf{X}_d$ is the nodal displacement vector with motions in three directions at each node $\mathbf{X}_{di} = [p_i \quad h_i \quad \alpha_i]^{\mathrm{T}}$ $(i = 1, \cdots, N)$, where N is the number of the nodes: the sway p_i, the hovering h_i and the pitching α_i. $\mathbf{F}^{se}$ and $\mathbf{F}^{b}$ are the vectors of self-excited forces and non-stationary/non-Gaussian buffeting forces, respectively, with the force components in three directions: the drag D^{se} and D^{b}, the lift L^{se} and L^{b}, and the torque M^{se} and M^{b}. Fig. 6 illustrates the motions of the bridge deck per unit length excited by aerodynamic forces.

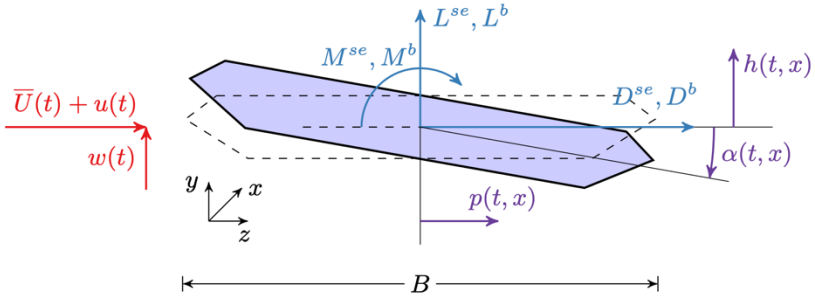

Fig. 6. Motions of bridge deck and aerodynamic forces in two dimensions.

4.2 Unsteady self-excited forces in time-domain

For harmonic motions of bridge decks, the motion-induced forces can be formulated by Scanlan's flutter derivatives (Scanlan, 1993) and equivalently expressed in the frequency domain

$$\begin{bmatrix} \bar{D}_i^{se} \\ \bar{L}_i^{se} \\ \bar{M}_i^{se} \end{bmatrix} = \frac{1}{2}\rho U^2 \Delta L \begin{bmatrix} K^2(P_4^* + \mathrm{j}P_1^*) & K^2(P_6^* + \mathrm{j}P_5^*) & K^2(P_3^* + \mathrm{j}P_2^*)B \\ K^2(H_6^* + \mathrm{j}H_5^*) & K^2(H_4^* + \mathrm{j}H_1^*) & K^2(H_3^* + \mathrm{j}H_2^*)B \\ K^2(A_6^* + \mathrm{j}A_5^*)B & K^2(A_4^* + \mathrm{j}A_1^*)B & K^2(A_3^* + \mathrm{j}A_2^*)B^2 \end{bmatrix} \begin{bmatrix} \bar{p}_i \\ \bar{h}_i \\ \bar{\alpha}_i \end{bmatrix} \tag{18}$$

where $\bar{h}_i$, $\bar{p}_i$ and $\bar{\alpha}_i$ are the complex-valued amplitudes of motions at the i-th node. $\bar{D}_i^{se}$, $\bar{L}_i^{se}$ and $\bar{M}_i^{se}$ are the complex-valued amplitudes of forces. $\rho = 1.25\ \mathrm{kg/m^3}$ is the air density. B is the deck width. ΔL is the element length. U is the mean wind speed. $K = \omega B/U$ is the reduced frequency, and ω is the circular frequency. H_i^*, P_i^* and A_i^* $(i = 1, 2, \cdots, 6)$ are the flutter derivatives. j is the imaginary unit. The study considers the variations in kinetic pressure and reduced frequencies induced by time-varying mean wind speeds. As the time scale of varying mean wind speeds is much larger than natural periods of structures, it is assumed that frequency-domain motion-induced forces still preserve the proportionality around the mean static position, and the slowly varying mean wind speed is regarded as being seemingly fixed when taking inverse Fourier transform to derive the time-domain forces in the following procedure. Notice that, as discussed in Section 2, great variations in wind directions and large-scale atmospheric turbulence can potentially result in large-amplitude low-frequency vertical turbulence, causing mean angles of attack to be slowly varying, as reported in (Fenerci and Øiseth, 2018). In the light of relatively small magnitudes of the system response and wind fluctuations compared to the mean wind speed, the variation in attack angles is currently disregarded in this study to give more focuses on the proposed methodology. In addition, as parametric excitations

related to wind fluctuations are not included, the perfectly spanwise coherence condition on kinetic pressure and flutter derivatives is maintained.

To facilitate transforming the motion-induced forces to time domain, the flutter derivatives are approximated in terms of rational functions known as Roger's approximation (Chen et al, 2000)

$$\begin{bmatrix} K^2(P_4^*+\mathrm{j}P_1^*) & K^2(P_6^*+\mathrm{j}P_5^*) & K^2(P_3^*+\mathrm{j}P_2^*)B \\ K^2(H_6^*+\mathrm{j}H_5^*) & K^2(H_4^*+\mathrm{j}H_1^*) & K^2(H_3^*+\mathrm{j}H_2^*)B \\ K^2(A_6^*+\mathrm{j}A_5^*)B & K^2(A_4^*+\mathrm{j}A_1^*)B & K^2(A_3^*+\mathrm{j}A_2^*)B^2 \end{bmatrix} = \mathbf{A}_{i,1}^{se} + \mathrm{j}K\mathbf{A}_{i,2}^{se} + (\mathrm{j}K)^2\mathbf{A}_{i,3}^{se} + \sum_{l=1}^{m_{se}} \frac{\mathrm{j}K\mathbf{A}_{i,l+3}^{se}}{\mathrm{j}K + d_l^{se}} \quad (19)$$

in which $\mathbf{A}_{i,1}^{se}$, $\mathbf{A}_{i,2}^{se}$, $\mathbf{A}_{i,3}^{se}$, $\mathbf{A}_{i,l+3}^{se}$ and $d_l^{se} \geq 0$ are frequency-independent coefficients, which can be determined by fitting rational functions to flutter derivatives using nonlinear least square method. The first three terms of the approximation represent the aerodynamic stiffness, damping and mass, respectively. The rational terms allow to consider the unsteady fluid memory effect, and m_{se} determines the level of accuracy of the approximation.

By means of rational function approximation, the unsteady forces induced by arbitrary motions can be easily obtained in the time domain by taking inverse Fourier-transform technique

$$\mathbf{F}^{se} = \frac{1}{2}\rho U^2 \Delta L \left(\mathbf{A}_1^{se}\mathbf{X}_d + \frac{B}{U}\mathbf{A}_2^{se}\dot{\mathbf{X}}_d + \frac{B^2}{U^2}\mathbf{A}_3^{se}\ddot{\mathbf{X}}_d + \sum_{l=1}^{m_{se}} \boldsymbol{\phi}_l^{se} \right) \quad (20a)$$

in which $\mathbf{A}_l^{se}$ is the partitioned diagonal matrix of $\mathbf{A}_{i,l}^{se}$ $(i = 1, \cdots, N)$, and $\boldsymbol{\phi}_l^{se}$ $(l = 1, \cdots, m_{se})$ are additional variables introduced to consider the unsteady effect and satisfy

$$\dot{\boldsymbol{\phi}}_l^{se} = -\frac{d_l^{se}U}{B}\boldsymbol{\phi}_l^{se} + \mathbf{A}_{l+3}^{se}\dot{\mathbf{X}}_d \quad (20b)$$

To extend the method to cases of varying mean angle of attack, it is expected to firstly obtain the low-frequency content of vertical turbulence given suitable cut-off frequency and then adopt a time-varying force model, as the pioneering work by (Barni and Mannini, 2024), resulting in the rational function coefficients A_l^{se} and d_l^{se} being functions of time. However, the proposed methodology is not substantially changed.

4.3 Non-stationary/non-Gaussian buffeting forces

As discussed in Section 2, the non-stationary feature and high turbulence intensity rarely occur at the same time. Therefore, the buffeting forces induced by these two types of non-synoptic winds are considered individually in the analysis.

The time-domain model of buffeting forces induced by non-stationary Gaussian turbulence can be obtained in an analogous way to motion-induced forces. Related study suggests that the frequency content in the EPSD of non-stationary fluctuations evolves rather slightly over time (Huang et al, 2015). A simplified uniformly modulated model is adopted to represent the non-stationary Gaussian wind fluctuations

$$u(t) = \beta_u(t)u^s(t) \quad (21a)$$

$$w(t) = \beta_w(t)w^s(t) \quad (21b)$$

in which $\beta_u(t)$ and $\beta_w(t)$ are the slowly varying time-modulation functions. Considering that the

substantial variations in non-synoptic wind features mainly result from large-scale circulations, as discussed in Section 2, therefore, the horizontal non-homogeneities of the wind field are disregarded on a bridge scale, and the time-varying mean wind speed and the time-modulation functions are assumed to be identical along the span.

$u^s(t)$ and $w^s(t)$ are the derived stationary Gaussian processes with zero means. Notice that the stationary wind fluctuations at different points are considered to be partially coherent by adopting an exponentially decaying coherent function in cross-spectra, and the wind auto-spectrum extracted from one-point wind measurement is uniformly applied along the bridge due to the horizontal homogeneity, as will be introduced in Section 4.4. These considerations are also applicable to the spatial wind features in the non-Gaussian force case.

The non-stationary buffeting force at the i-th node $\mathbf{F}_i^b$ is expressed as

$$\mathbf{F}_i^b = \beta^u \mathbf{F}_i^{bu} + \beta^w \mathbf{F}_i^{bw} \tag{22}$$

in which $\mathbf{F}_i^{bu}$ and $\mathbf{F}_i^{bw}$ are the buffeting forces induced by longitudinal and vertical stationary wind fluctuations, respectively, given by

$$\mathbf{F}_i^{bu} = \frac{1}{2}\rho U \Delta L \begin{bmatrix} 2BC_D\chi_{D_u} \\ 2BC_L\chi_{L_u} \\ 2B^2C_M\chi_{M_u} \end{bmatrix} u_i^s = \frac{1}{2}\rho U \Delta L \boldsymbol{\chi}_i^u u_i^s \tag{23a}$$

$$\mathbf{F}_i^{bw} = \frac{1}{2}\rho U \Delta L \begin{bmatrix} B(C_D' - C_L)\chi_{D_w} \\ B(C_L' + C_D)\chi_{L_w} \\ B^2C_M'\chi_{M_w} \end{bmatrix} w_i^s = \frac{1}{2}\rho U \Delta L \boldsymbol{\chi}_i^w w_i^s \tag{23b}$$

in which u_i^s and w_i^s are complex-valued sinusoidal oscillations at the i-th node. χ_{D_u}, χ_{D_w}, χ_{L_u}, χ_{L_w}, χ_{M_u} and χ_{M_w} are aerodynamic admittances. C_D, C_L and C_M are drag, lift and pitching torque coefficients, respectively. C_D', C_L' and $C_M'$are their derivatives around the static wind attack angle. $\boldsymbol{\chi}_i^u$ and $\boldsymbol{\chi}_i^w$ are the vectors of force coefficients and admittance functions and can be approximated as rational functions in an analogous way to flutter derivatives

$$\boldsymbol{\chi}_i^u = \mathbf{A}_{i,1}^u + \sum_{l=1}^{m_u} \frac{\mathrm{j}K\mathbf{A}_{i,l+1}^u}{\mathrm{j}K + d_l^u} \tag{24}$$

in which $\mathbf{A}_{i,1}^u$, $\mathbf{A}_{i,l+1}^u$ and $d_l^u \geq 0$ are frequency-independent coefficients. By means of this, the buffeting forces in the time domain are obtained by taking inverse Fourier-transform technique

$$\mathbf{F}^{bu} = \frac{1}{2}\rho U \Delta L \sum_{l=1}^{m_u+1} \mathbf{A}_l^u \, \mathbf{u}^s - \frac{1}{2}\rho U \Delta L \sum_{l=1}^{m_u} \frac{d_l^u U}{B} \boldsymbol{\phi}_l^u \tag{25a}$$

in which $\mathbf{A}_l^u$ is the partitioned diagonal matrix of $\mathbf{A}_{i,l}^u$ $(i = 1, \cdots, N)$, and $\mathbf{u}^s$ is the stationary along-wind fluctuations. $\boldsymbol{\phi}_l^u$ $(l = 1, \cdots, m_u)$ are additional variables that satisfy

$$\dot{\boldsymbol{\phi}}_l^u = -\frac{d_l^u U}{B} \boldsymbol{\phi}_l^u + \mathbf{A}_{l+1}^u \mathbf{u}^s \tag{25b}$$

Notice that similar formulas for buffeting forces induced by crosswind fluctuations are omitted for the

sake of brevity. The non-stationary Gaussian buffeting forces in Eq. (17) are thus expressed as

$$\mathbf{F}^b = \beta^u \mathbf{F}^{bu} + \beta^w \mathbf{F}^{bw} \tag{26}$$

Due to the high turbulence intensity, the quadratic terms of turbulences in buffeting forces become significant and cannot be understated, leading to the non-Gaussian characteristic of excitations. Notice that the admittance functions are introduced to consider the unsteady effect of Gaussian buffeting forces that are in linear relation to turbulence, as a correction function to quasi-steady assumption. However, there hasn't been such a correction function dedicated to buffeting forces in the presence of quadratic terms of turbulences. Thus, the buffeting forces induced by high-intensity turbulences are modeled by the simple expedient of invoking the quasi-steady assumption.

Based on the geometric relations from Fig. 2, the instantaneous relative angle of attack α_i^e and the relative wind velocity U_i^e that are related to the turbulences per se are given as

$$\alpha_i^e(t) = \alpha_i^0 + \psi_i(t) \approx \alpha_i^0 + \frac{w_i(t)}{U} \tag{27}$$

$$U_i^{e\,2} = (U + u_i)^2 + w_i^2 \tag{28}$$

in which α_i^0 is the attack angle in the equilibrium position and ψ_i is the varying part induced by turbulence per se.

According to the quasi-steady theory, with the quadratic terms from the geometric relations and the curvature of the aerodynamic coefficients retained (Denoël and Degée, 2006), the non-Gaussian buffeting forces in the instantaneous wind reference system are derived as

$$\begin{bmatrix} F_{Di}^b \\ F_{Li}^b \\ F_{Mi}^b \end{bmatrix} = \frac{1}{2}\rho B \Delta L U_i^{e\,2} \begin{bmatrix} C_D(\alpha_i^e) \\ C_L(\alpha_i^e) \\ BC_M(\alpha_i^e) \end{bmatrix} \approx \frac{1}{2}\rho B \Delta L (U^2 + 2Uu_i + u_i^2 + w_i^2) \begin{bmatrix} C_D + C_D'\psi_i + \frac{1}{2}C_D''\psi_i^2 \\ C_L + C_L'\psi_i + \frac{1}{2}C_L''\psi_i^2 \\ B\left(C_M + C_M'\psi_i + \frac{1}{2}C_M''\psi_i^2\right) \end{bmatrix} \tag{29}$$

The buffeting forces are then transformed to the global coordinate aligned with mean wind speed by referring to the geometric relations

$$\mathbf{F}_i^b = \begin{bmatrix} F_{zi}^b \\ F_{yi}^b \\ F_{\alpha i}^b \end{bmatrix} = \begin{bmatrix} F_{Di}^b \cos\psi_i - F_{Li}^b \sin\psi_i \\ F_{Di}^b \sin\psi_i + F_{Li}^b \cos\psi_i \\ F_{Mi}^b \end{bmatrix} \tag{30}$$

The buffeting forces $\mathbf{F}^b$ in the global coordinate are finally written as

$$\mathbf{F}^b = \mathbf{F}^{bu} + \mathbf{F}^{bw} + \mathbf{F}^{buu} + \mathbf{F}^{buw} + \mathbf{F}^{bww} \tag{31}$$

in which $\mathbf{F}^{bu}$ and $\mathbf{F}^{bw}$ are the force components connected with linear terms u and w. $\mathbf{F}^{buu}$ and $\mathbf{F}^{bww}$ are the components connected with quadratic terms u^2 and w^2, and $\mathbf{F}^{buw}$ is the component contributed by the cross term uw. It will be shown in the next section that the component-wise expression of non-Gaussian buffeting forces will facilitate the polynomial approximation to OU processes. The detailed expressions of these components are given in Appendix E. Notice that their

mean values are deducted to facilitate the stochastic dynamic analysis.

4.4 State-space equations in modal coordinates

Based on superposition principle, the system responses can be expressed in the modal-amplitude coordinate, i.e., $\mathbf{X}_d = \boldsymbol{\Psi}\mathbf{q}$, in which $\boldsymbol{\Psi}$ is the matrix of mode shapes and $\mathbf{q}$ is the modal coordinate vector with n modes interested. The generalized equation of motion is derived as

$$\mathbf{M}_q\ddot{\mathbf{q}} + \mathbf{C}_q\dot{\mathbf{q}} + \mathbf{K}_q\mathbf{q} = \mathbf{Q}^{se} + \mathbf{Q}^{b} \tag{32}$$

in which $\mathbf{M}_q = \boldsymbol{\Psi}^{\mathrm{T}}\mathbf{M}_d\boldsymbol{\Psi}$, $\mathbf{C}_q = \boldsymbol{\Psi}^{\mathrm{T}}\mathbf{C}_d\boldsymbol{\Psi}$ and $\mathbf{K}_q = \boldsymbol{\Psi}^{\mathrm{T}}\mathbf{K}_d\boldsymbol{\Psi}$ are the modal mass, damping and stiffness matrices, respectively. $\mathbf{Q}^{se} = \boldsymbol{\Psi}^{\mathrm{T}}\mathbf{F}^{se}$ is the generalized motion-induced force vector. $\mathbf{Q}^{b}$ is the generalized buffeting force vector.

In the case of non-stationary winds, $\mathbf{Q}^{b} = \beta^{u}\boldsymbol{\Psi}^{\mathrm{T}}\mathbf{F}^{bu} + \beta^{w}\boldsymbol{\Psi}^{\mathrm{T}}\mathbf{F}^{bw}$. The generalized equation of motion is transformed to its state-space form

$$\dot{\mathbf{Y}} = \boldsymbol{\mathcal{A}}(t)\mathbf{Y} + \boldsymbol{\mathcal{B}}_u(t)\mathbf{u}^{s,q} + \boldsymbol{\mathcal{B}}_w(t)\mathbf{w}^{s,q} \tag{33}$$

in which $\mathbf{Y} = \left[\mathbf{q}^{\mathrm{T}} \quad \dot{\mathbf{q}}^{\mathrm{T}} \quad \mathbf{q}_1^{se\,\mathrm{T}} \quad \cdots \quad \mathbf{q}_{m_{se}}^{se\,\mathrm{T}} \quad \mathbf{q}_1^{u\,\mathrm{T}} \quad \cdots \quad \mathbf{q}_{m_u}^{u\,\mathrm{T}} \quad \mathbf{q}_1^{w\,\mathrm{T}} \quad \cdots \quad \mathbf{q}_{m_w}^{w\,\mathrm{T}}\right]^{\mathrm{T}}$ is the state vector. $\mathbf{q}_l^{se} = \boldsymbol{\Psi}^{\mathrm{T}}\boldsymbol{\phi}_l^{se}$, $\mathbf{q}_l^{u} = \boldsymbol{\Psi}^{\mathrm{T}}\boldsymbol{\phi}_l^{u}$ and $\mathbf{q}_l^{w} = \boldsymbol{\Psi}^{\mathrm{T}}\boldsymbol{\phi}_l^{w}$ are the generalized additional variables to consider unsteady effects of the aerodynamic forces. $\boldsymbol{\mathcal{A}}(t)$, $\boldsymbol{\mathcal{B}}_u(t)$ and $\boldsymbol{\mathcal{B}}_w(t)$ are the time-varying coefficient matrices, of which the detailed expressions are given in Appendix F. $\mathbf{u}^{s,q} = \mathbf{A}^{u,q}\mathbf{u}^{s}$ and $\mathbf{w}^{s,q} = \mathbf{A}^{w,q}\mathbf{w}^{s}$ are the generalized stationary pseudo-fluctuations in which $\mathbf{A}^{u,q} = \left[\mathbf{A}_1^{u\,\mathrm{T}}\boldsymbol{\Psi} \quad \cdots \quad \mathbf{A}_{m_u+1}^{u\,\mathrm{T}}\boldsymbol{\Psi}\right]^{\mathrm{T}}$ and $\mathbf{A}^{w,q} = \left[\mathbf{A}_1^{w\,\mathrm{T}}\boldsymbol{\Psi} \quad \cdots \quad \mathbf{A}_{m_w+1}^{w\,\mathrm{T}}\boldsymbol{\Psi}\right]^{\mathrm{T}}$. The spectral density matrices for $\mathbf{u}^{s,q}$ and $\mathbf{w}^{s,q}$ are given by

$$\mathbf{S}_{\mathbf{u}^{s,q}} = S_u\mathbf{A}^{u,q}\boldsymbol{\mathcal{C}}_{\mathbf{u}}(\mathbf{A}^{u,q})^{\mathrm{T}} \tag{34a}$$

$$\mathbf{S}_{\mathbf{w}^{s,q}} = S_w\mathbf{A}^{w,q}\boldsymbol{\mathcal{C}}_{\mathbf{w}}(\mathbf{A}^{w,q})^{\mathrm{T}} \tag{34b}$$

in which $\boldsymbol{\mathcal{C}}_{\mathbf{u}}$ and $\boldsymbol{\mathcal{C}}_{\mathbf{w}}$ are the matrices of time-invariant coherence functions to describe the partially coherent wind fluctuations at two points in space, as discussed in Section 4.3. The exponentially decaying law is invoked to describe their spatial coherence, with the decay coefficients $c_u = 16$ for longitudinal turbulence and $c_w = 8$ for vertical turbulence. The detailed expressions of $\boldsymbol{\mathcal{C}}_{\mathbf{u}}$ and $\boldsymbol{\mathcal{C}}_{\mathbf{w}}$ are given in Appendix F, and also applicable to the non-Gaussian force case. S_u and S_w are the longitudinal and vertical wind spectra, respectively, which are assumed to be identical along the span due to the horizontal homogeneity assumption. Notice that the correlations between the wind components in two directions are disregarded in this study.

In the case of high turbulence intensity, $\mathbf{Q}^{b} = \mathbf{Q}^{bu} + \mathbf{Q}^{bw} + \mathbf{Q}^{buu} + \mathbf{Q}^{buw} + \mathbf{Q}^{bww}$ where the generalized buffeting force components are given as, for instance, $\mathbf{Q}^{bu} = \boldsymbol{\Psi}^{\mathrm{T}}\mathbf{F}^{bu}$. The generalized equation of motion is transformed to its state-space form

$$\dot{\mathbf{Y}} = \boldsymbol{\mathcal{A}}\mathbf{Y} + \boldsymbol{\mathcal{B}}\mathbf{Q}^{b} \tag{35}$$

in which $\mathbf{Y} = \left[\mathbf{q}^{\mathrm{T}} \quad \dot{\mathbf{q}}^{\mathrm{T}} \quad \mathbf{q}_1^{se\,\mathrm{T}} \quad \cdots \quad \mathbf{q}_{m_{se}}^{se\,\mathrm{T}}\right]^{\mathrm{T}}$ is the state vector. $\boldsymbol{\mathcal{A}}$ and $\boldsymbol{\mathcal{B}}$ are the time-invariant coefficient matrices, of which the detailed expressions are given in Appendix F. According to Isserlis'

theorem, the spectral density matrix for $\mathbf{Q}^b$ is given by

$$\mathbf{S}_{\mathbf{Q}^b\mathbf{Q}^b} = \mathbf{S}_{\mathbf{Q}^{bu}\mathbf{Q}^{bu}} + \mathbf{S}_{\mathbf{Q}^{bw}\mathbf{Q}^{bw}} + \mathbf{S}_{\mathbf{Q}^{buu}\mathbf{Q}^{buu}} + \mathbf{S}_{\mathbf{Q}^{bww}\mathbf{Q}^{bww}} + \mathbf{S}_{\mathbf{Q}^{buw}\mathbf{Q}^{buw}} \tag{36}$$

in which the spectral density functions of linear terms are derived as

$$\mathbf{S}_{\mathbf{Q}^{bu}\mathbf{Q}^{bu}} = \left(\frac{1}{2}\rho B\Delta LU\right)^2 \mathbf{\Psi}^{\mathrm{T}}\mathbf{A}^{u}\mathbf{S}_{\mathbf{u}}\mathbf{A}^{u\mathrm{T}}\mathbf{\Psi} \tag{37a}$$

$$\mathbf{S}_{\mathbf{Q}^{bw}\mathbf{Q}^{bw}} = \left(\frac{1}{2}\rho B\Delta LU\right)^2 \mathbf{\Psi}^{\mathrm{T}}\mathbf{A}^{w}\mathbf{S}_{\mathbf{w}}\mathbf{A}^{w\mathrm{T}}\mathbf{\Psi} \tag{37b}$$

By applying convolution technique, the spectral density functions of quadratic terms are derived as

$$\mathbf{S}_{\mathbf{Q}^{buu}\mathbf{Q}^{buu}} = \left(\frac{1}{2}\rho B\Delta L\right)^2 \mathbf{\Psi}^{\mathrm{T}}\mathbf{A}^{uu}\left(\frac{1}{\pi}\int_{-\infty}^{\infty}\mathbf{S}_{\mathbf{u}}(\omega')\mathbf{S}_{\mathbf{u}}(\omega-\omega')\mathrm{d}\omega'\right)\mathbf{A}^{uu\mathrm{T}}\mathbf{\Psi} \tag{37c}$$

$$\mathbf{S}_{\mathbf{Q}^{bww}\mathbf{Q}^{bww}} = \left(\frac{1}{2}\rho B\Delta L\right)^2 \mathbf{\Psi}^{\mathrm{T}}\mathbf{A}^{ww}\left(\frac{1}{\pi}\int_{-\infty}^{\infty}\mathbf{S}_{\mathbf{w}}(\omega')\mathbf{S}_{\mathbf{w}}(\omega-\omega')\mathrm{d}\omega'\right)\mathbf{A}^{ww\mathrm{T}}\mathbf{\Psi} \tag{37d}$$

$$\mathbf{S}_{\mathbf{Q}^{buw}\mathbf{Q}^{buw}} = \left(\frac{1}{2}\rho B\Delta L\right)^2 \mathbf{\Psi}^{\mathrm{T}}\mathbf{A}^{uw}\left(\frac{1}{2\pi}\int_{-\infty}^{\infty}\mathbf{S}_{\mathbf{u}}(\omega')\mathbf{S}_{\mathbf{w}}(\omega-\omega')\mathrm{d}\omega'\right)\mathbf{A}^{uw\mathrm{T}}\mathbf{\Psi} \tag{37e}$$

where $\mathbf{S}_{\mathbf{u}} = S_u\boldsymbol{\mathcal{C}}_{\mathbf{u}}$ and $\mathbf{S}_{\mathbf{w}} = S_w\boldsymbol{\mathcal{C}}_{\mathbf{w}}$, of which the detailed expressions are given in Appendix F.

4.5 Statistical moment equations of non-stationary buffeting responses

As mentioned in Section 3.2, the stationary processes can be approximated as polynomials of Ornstein-Uhlenbeck processes. In the case of non-stationary winds, the generalized stationary pseudo-fluctuations are approximated as $\mathbf{u}^{s,q} \approx \mathbf{Z}^{u}$ and $\mathbf{w}^{s,q} \approx \mathbf{Z}^{w}$, so the augmented states of the system and the excitations are written as

$$\mathrm{d}\begin{bmatrix}\mathbf{Y}\\ \mathbf{Z}^{u}\\ \mathbf{Z}^{w}\end{bmatrix} = \begin{bmatrix}\boldsymbol{\mathcal{A}} & \boldsymbol{\mathcal{B}}_u & \boldsymbol{\mathcal{B}}_w\\ \mathbf{0} & -\boldsymbol{\alpha}^{u} & \mathbf{0}\\ \mathbf{0} & \mathbf{0} & -\boldsymbol{\alpha}^{w}\end{bmatrix}\begin{bmatrix}\mathbf{Y}\\ \mathbf{Z}^{u}\\ \mathbf{Z}^{w}\end{bmatrix}\mathrm{d}t + \begin{bmatrix}\mathbf{0} & \mathbf{0}\\ \boldsymbol{\Theta}^{u} & \mathbf{0}\\ \mathbf{0} & \boldsymbol{\Theta}^{w}\end{bmatrix}\mathrm{d}\begin{bmatrix}\mathbf{W}^{u}\\ \mathbf{W}^{w}\end{bmatrix} \tag{38}$$

In the case of high turbulence intensity, the non-Gaussian excitations are approximated as $\mathbf{Q}^b = \sum_{j=1}^{k}\mathbf{\Gamma}_j\mathrm{diag}(\mathbf{Z}^{Q})^{j-1}\mathbf{Z}^{Q}$, so the augmented states of the system and the excitations are written as

$$\mathrm{d}\begin{bmatrix}\mathbf{Y}\\ \mathbf{Z}^{Q}\end{bmatrix} = \begin{bmatrix}\boldsymbol{\mathcal{A}} & \boldsymbol{\mathcal{B}}\sum_{j=1}^{k}\mathbf{\Gamma}_j\mathrm{diag}(\mathbf{Z}^{Q})^{j-1}\\ \mathbf{0} & -\boldsymbol{\alpha}^{Q}\end{bmatrix}\begin{bmatrix}\mathbf{Y}\\ \mathbf{Z}^{Q}\end{bmatrix}\mathrm{d}t + \begin{bmatrix}\mathbf{0}\\ \boldsymbol{\Theta}^{Q}\end{bmatrix}\mathrm{d}\mathbf{W}^{Q} \tag{39}$$

in which $\boldsymbol{\alpha}^{u}$, $\boldsymbol{\Theta}^{u}$, $\boldsymbol{\alpha}^{w}$, $\boldsymbol{\Theta}^{w}$, $\boldsymbol{\alpha}^{Q}$ and $\boldsymbol{\Theta}^{Q}$ are the corresponding coefficients of OU processes, and $\mathbf{W}^{u}$, $\mathbf{W}^{w}$ and $\mathbf{W}^{Q}$ are the Wiener processes.

Depending on the wind input characteristics, the two distinct augmented state equations should be alternatively used and then fitted into the Itô-type stochastic differential equation, as reported by Eq. (7). The corresponding expressions in accordance with Eq. (38) or Eq. (39) are given in Appendix F. By following the procedure demonstrated in Section 3.3, the statistical moment equation can easily be obtained as a first-order differential equation with the same form as Eq. (14).

5 Numerical applications

5.1 Bridge description

As an illustration of the application of the state augmentation method (SAM), the proposed method is applied to calculate the buffeting responses of a model bridge during the passage of Typhoon Hagupit, of which the time history is shown in Fig. 1. The bridge has a main span of 1666 m and the deck of 49.7 m in width, which is geometrically illustrated in Fig. 7. To show the ability of the proposed method, the first symmetric torsional mode together with all the prior (three in total) symmetric vertical modes is considered, of which the modal shapes and frequencies are based on modal analysis results. The flutter derivatives adopted in the analysis are those obtained in the wind tunnel experiment (Lin et al, 2019). Table 2 lists the main structural and aerodynamic parameters of the bridge. Notice that this study considers the bridge model in construction stage, where the bridge hasn't been loaded with deck pavement and facilities. This gives different structural dynamic characteristics and aerodynamic parameters compared to the model used in (Xu et al, 2023).

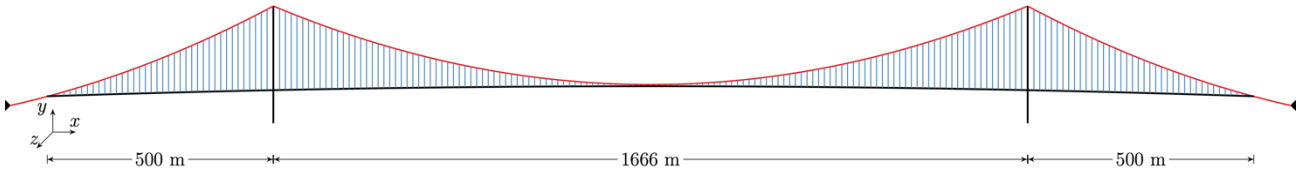

Fig. 7. Model of the long-span suspension bridge (in-construction stage).

Table 2. Structural dynamic characteristics and aerodynamic parameters of the bridge (in-construction stage).

Parameter	Definition	Unit	Value
L	Main span	m	1666
B	Deck width	m	49.7
M	Mass per unit length	kg/m	14122
I	Moment of inertia per unit length	$\mathrm{kg \cdot m^2/m}$	2.32×10^6
ξ	Structural damping ratio	/	0.005
ρ	Air density	$\mathrm{kg/m^3}$	1.25
n_1^{SV}	Modal frequency of 1st symmetric vertical mode	Hz	0.1049
n_2^{SV}	Modal frequency of 2nd symmetric vertical mode	Hz	0.1366
n_3^{SV}	Modal frequency of 3rd symmetric vertical mode	Hz	0.2256
n_1^{ST}	Modal frequency of 1st symmetric torsional mode	Hz	0.2987
C_D	Drag coefficient at zero-degree attack angle	/	0.825
C_L	Lift coefficient at zero-degree attack angle	/	−0.048
C_M	Moment coefficient at zero-degree attack angle	/	0.011
C_D'	Derivative of drag coefficient at zero-degree attack angle	/rad	0.207
C_L'	Derivative of lift coefficient at zero-degree attack angle	/rad	3.158
C_M'	Derivative of moment coefficient at zero-degree attack angle	/rad	0.367

The reliability and computing effort of the proposed state augmentation method have been well validated in the preceding published research by the authors, as referenced to the non-stationary case in (Lei et al, 2022a) and to the non-Gaussian and high turbulence intensity cases in (Zhang et al, 2023). For the sake of brevity, the validation is not repeated in the study. Through comparing to the results obtained by using the available methods, such as frequency domain method (FDM) and pseudo excitation method (PEM) (Jones and Scanlan, 2001), the proposed approach showed great reliability and efficiency.

An essential part of the SAM is the calibration of the coefficient matrices $\boldsymbol{\alpha}$ and $\boldsymbol{\Theta}$ so that the stationary Gaussian processes, e.g., $\mathbf{u}^{s,q}$, can be well-represented by OU processes, e.g., $\mathbf{Z}^u$. As the total buffeting response is mainly dominated by background response and resonant response, which is due to the narrow-band characteristic of the mechanical transfer function around the system natural frequencies, while calibrating the values of $\boldsymbol{\alpha}$ and $\boldsymbol{\Theta}$, the covariance matrix $\mathbf{K}_{\mathbf{Z}^u\mathbf{Z}^u}$ of $\mathbf{Z}^u$ is supposed to remain the same as the one of $\mathbf{u}^{s,q}$

$$\mathbf{K}_{\mathbf{Z}^u\mathbf{Z}^u} = \int_{n_1}^{n_2} \mathbf{S}_{\mathbf{u}^{s,q}} \mathrm{d}n \tag{40}$$

in which n_1 and n_2 are cut-off frequencies. Then $\boldsymbol{\alpha}$ can be found through minimizing the differences between $\mathbf{S}_{\mathbf{u}^{s,q}}$ and $\mathbf{S}_{\mathbf{Z}^u}$ at the concerned natural frequencies. By adopting the effective optimization algorithm combined with the clustering method, the target auto-spectra and cross-spectra containing the coherence feature are well fitted. Notice that the aerodynamic stiffness changes the system modal pattern, so the target spectra should be fitted in accordance with overall on-wind modal frequencies. Finally, $\boldsymbol{\Theta}$ is determined by solving the Lyapunov equation reported by Eq. (5). For instance, the calibration result and the comparison of $\mathbf{S}_{\mathbf{u}^{s,q}}$ and $\mathbf{S}_{\mathbf{Z}^u}$ in the case of wind Segment No. 138 are given in Fig. 8.

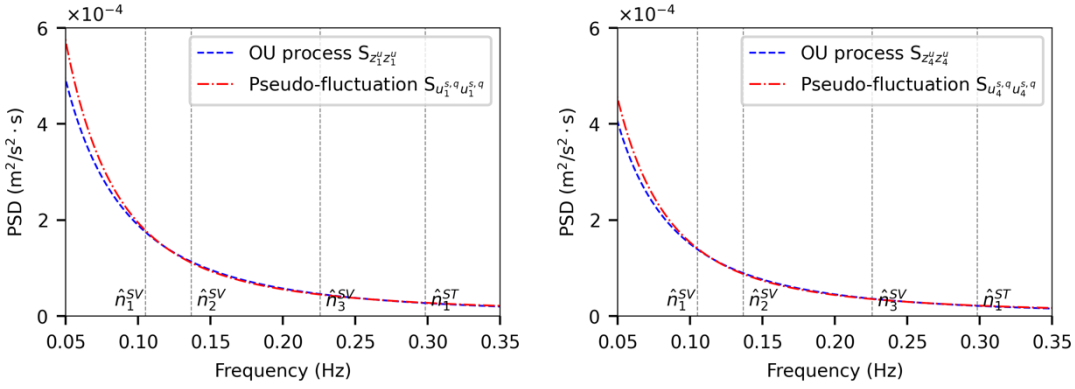

(a) (b)

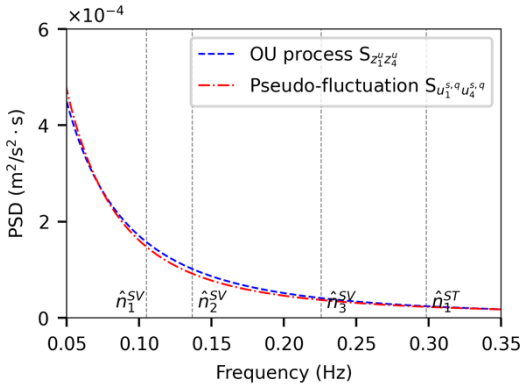

(c)

Fig. 8. Comparison between spectral density matrices of the generalized longitudinal stationary pseudo-fluctuations $\mathbf{u}^{s,q}$ and the fitted OU processes $\mathbf{Z}^u$ with vertical reference lines representing overall on-wind modal frequencies: (a) auto-spectra of $u_1^{s,q}$ and Z_1^u; (b) auto-spectra of $u_4^{s,q}$ and Z_4^u; (c) cross-spectra of $u_1^{s,q}$ and $u_4^{s,q}$, and of Z_1^u and Z_4^u.

5.2 Buffeting responses to wind Segments No. 138 and No. 69

Two representative wind segments (No. 138 and No. 69) are selected from the wind record to conduct the buffeting analysis, of which the detailed results are provided in the following, as an illustration of the non-stationary feature (induced by Segment No. 138) and non-Gaussian feature (induced by Segment No. 69) of buffeting responses induced by non-synoptic winds. Notice that a summary of buffeting responses to all wind segments will be provided in Section 5.3. The bridge is assumed initially at rest when subjected to each segment of the wind. Besides, as a comparison, the conventional frequency domain method (FDM) is employed to calculate the stationary response by assuming the wind speed as stationary within each segment and calculating the response PSD over 500 frequency points.

Fig. 9 (a) and (b) show the RMS results of the vertical and rotational displacements of the bridge deck at the mid-span for wind Segment No. 138, along with the amplification coefficients of the time-varying RMS to the stationary one. Table 3 reports the corresponding extreme responses under non-stationary and stationary assumptions (Chen, 2015) and their amplification coefficients. The expected extreme values of non-stationary response are evaluated based on the approach proposed in (Huang et al, 2013)

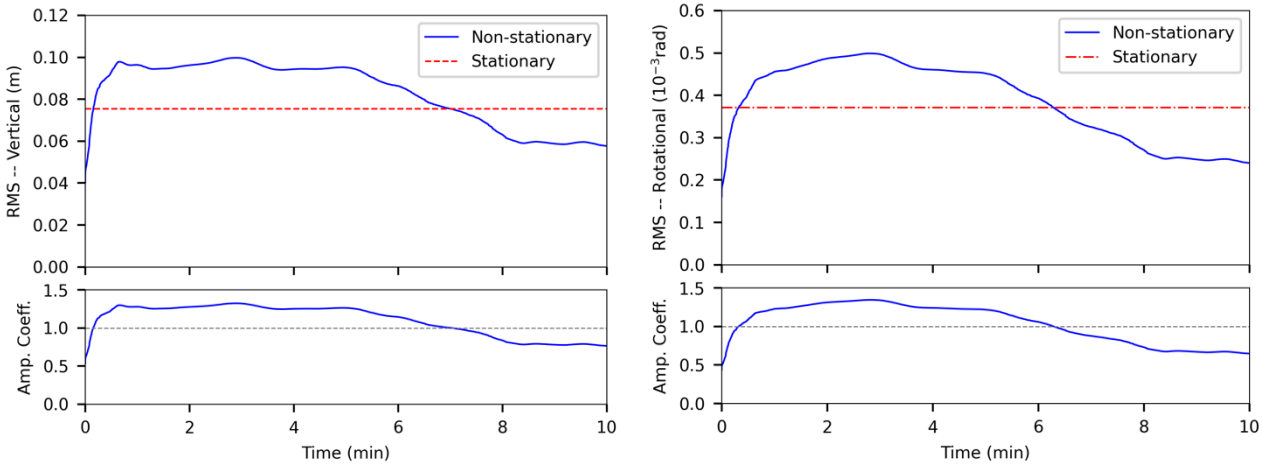

(a) (b)

Fig. 9. Time-varying RMS of displacement responses of the bridge deck at the mid-span under excitations of wind Segment No. 138: (a) vertical displacement; (b) rotational displacement.

Table 3. Comparison of extreme values of non-stationary and stationary responses.

Extreme responses	Vertical disp.	Torsional disp.
Non-stationary	0.297 m	0.0021 rad
Stationary	0.224 m	0.0015 rad
Amplification Coeff.	1.33	1.4

The computational efficiency of the proposed method is much higher than that of FDM. An Intel Core i7 4-Core computer with a main frequency of up to 3.4 GHz and 16 GB RAM is used in this study. The computing time taken by the SAM is about 219 s, and the time taken by the FDM is around 6724 s (without parallel computing). Notice that the computational effort for the FDM is largely spent in calculating the response PSD at discrete frequencies, and so the total running time is roughly in proportion to the frequency number. In contrast, with the SAM, the response moments are directly calculated by solving the moment equations once only, which would offer more significant advantages when applied to problems with high degrees of freedom. As seen from Fig. 9, the RMS responses vary considerably with time, presenting remarkable non-stationary feature. Moreover, the trend in the variation is found similar to that of the corresponding mean wind speed, as shown in Fig. 3 (b). As the time-varying mean wind speed plays as the coefficient of the buffeting force, this has a direct result in amplifying or abating the intensity of the excitations. This also happens to the motion-induced force, causing the consequent variation in the aerodynamic damping, which may partially account for the similarity in the trends.

In addition, great discrepancies are observed between the non-stationary response and stationary response. The initial responses from the non-stationary results are always found to be lower than the stationary ones, partly due to its lack of "build-up" time to reach a stationary state, as has been reported by several papers (Chen, 2008; Huang et al, 2013). However, as the energy begins to accumulate, the

peak of the non-stationary response is gradually rising and finally exceeds the stationary results, for the stationary assumption disregards the peak of the non-stationary excitations. As a result, the simple stationarity treatment may fail to capture the true peak response and thus lead to risks in terms of extreme responses as reported in Table 3 (Lei et al, 2022a).

Table 4 presents the RMS results of vertical and rotational displacements of the bridge deck at the mid-span, excited by non-Gaussian and Gaussian buffeting forces indued by wind Segment No. 69, along with the amplification coefficients of the non-Gaussian RMS to the Gaussian one. It is crucial to assess the influence of quadratic terms on the skewness and kurtosis of non-Gaussian responses, which are thereby presented in Table 5. Since the skewness and kurtosis of stationary responses are constant values, i.e., 0 and 3 respectively, they are omitted in Table 5. Furthermore, Table 6 reports the peak factors and expected extreme values for both non-Gaussian (Gurley et al, 1997) and Gaussian responses and the amplification coefficients of extreme values.

Table 4. RMS values of vertical and rotational responses to non-Gaussian and Gaussian excitations.

RMS responses	Vertical disp.	Torsional disp.
Non-Gaussian	0.14 m	0.001 rad
Gaussian	0.139 m	0.00098 rad
Amplification Coeff.	1.01	1.04

Table 5. High-order standardized statistical moments of non-Gaussian responses.

Standardized statistics	Vertical disp.	Torsional disp.
Skewness	0.03	0.09
Kurtosis	3.03	3.2

Table 6. Peak factors, gust factors and extreme values of non-Gaussian and Gaussian responses.

Quantities	Vertical disp.	Torsional disp.
Peak factor (NG)	3.15	3.78
Peak factor (G)	3.08	3.4
Extreme response (NG)	0.424 m	0.0046 rad
Extreme response (G)	0.409 m	0.0039 rad
Amplification Coeff.	1.04	1.18

Table 4 reveals that the inclusion of quadratic terms in buffeting forces has a limited impact on RMS responses. As suggested in (Zhang et al, 2023), these terms tend to exert a more pronounced impact on RMS responses under high mean wind speeds. However, in Segment No. 69, the mean wind speed remains relatively moderate, around 16.4 m/s. Despite this, a noticeable increase in extreme responses appears in torsional displacement, as reported in Table 6. This significant amplification mainly arises from the substantial influence of quadratic terms on the non-Gaussian characteristics of the responses, resulting in an increased kurtosis (as shown in Table 5) and a larger peak factor. Although the disregard of quadratic terms under strong turbulence might not significantly affect RMS

responses, it may underestimate extreme responses in specific scenarios, thereby posing potential design risks.

5.3 Buffeting responses during passage of Typhoon Hagupit

In this section, the proposed state augmentation method is employed to conduct a comprehensive buffeting analysis of the model bridge, considering all wind segments of Typhoon Hagupit, of which the longitudinal wind history with its statistical information in Section 2. Fig. 10 summarizes the maximal RMS responses at the mid-span for each segment under non-stationary/non-Gaussian assumptions with comparisons to their stationary/Gaussian counterparts. Additionally, a comparison of the corresponding expected extreme responses is provided in Fig. 11.

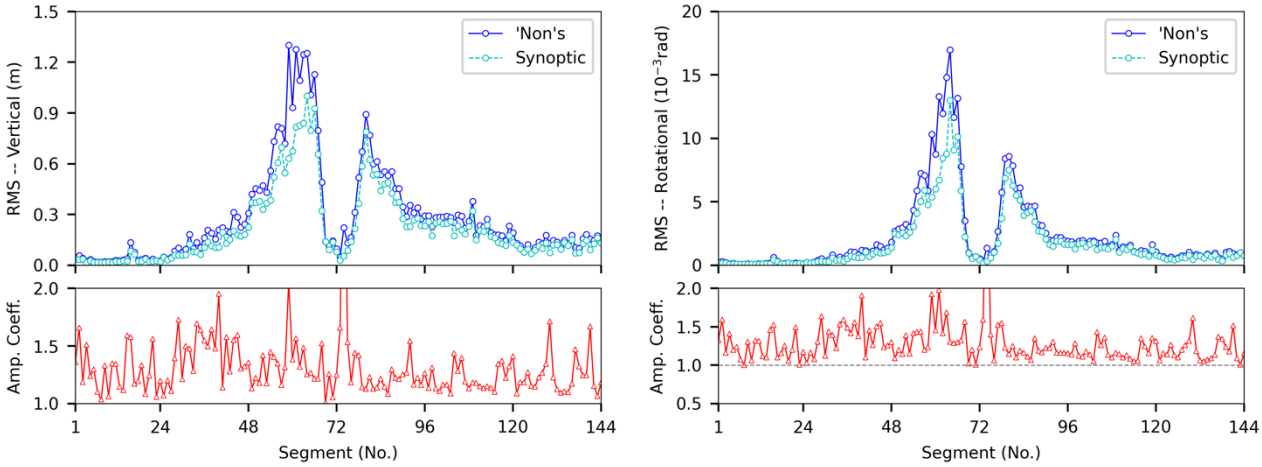

(a) (b)

Fig. 10. Comparison of RMS responses of the model bridge to non-stationary/non-Gaussian and stationary/Gaussian excitations induced by all wind segments of Typhoon Hagupit: (a) vertical displacement; (b) rotational displacement.

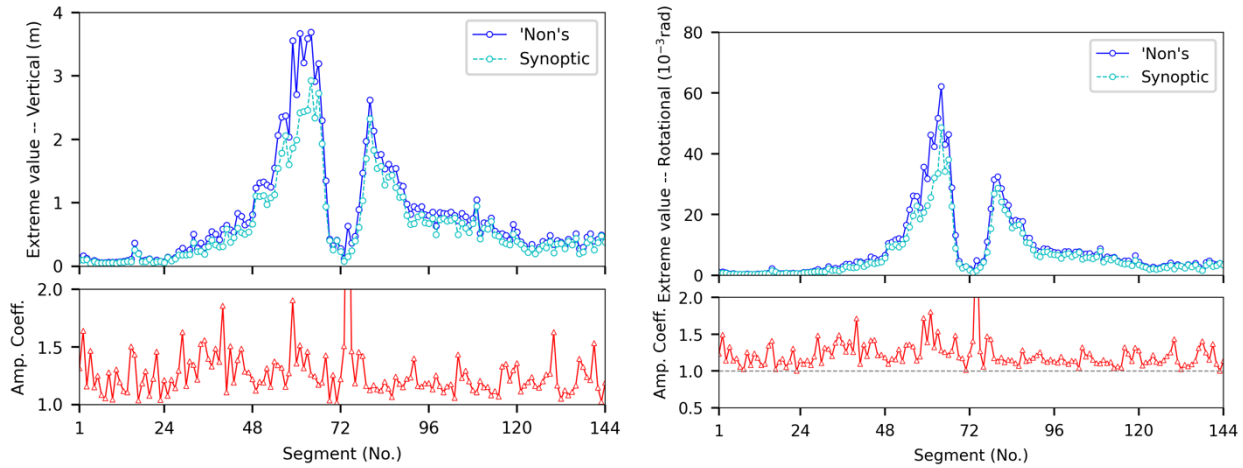

(a) (b)

Fig. 11. Expected extreme responses of the model bridge to non-stationary/non-Gaussian and stationary/Gaussian excitations induced by all wind segments of Typhoon Hagupit: (a) vertical

displacement; (b) rotational displacement.

As demonstrated in Figures 10 and 11, the maximal RMS and extreme values of the vertical and rotational responses exhibit significant variation across the wind segments. This variation closely mirrors the trend in segmented mean wind speeds reported in Fig. 2. Notably, during the passage of the typhoon eye between the 10th and 14th hours (Segments No. 60 to 84), the observation site experienced drastic changes in wind direction and speed, with nearly a $180°$ change in direction after landfall. Both the peak extreme values for vertical and rotational responses are observed in Segment No. 64, where the highest recorded mean wind speed of 46 m/s is found. The deterministic flutter stability examination is further conducted on the bridge, showing the critical wind speed of flutter instability at 97 m/s, which implies its very good rotational stability during Typhoon Hagupit where the wind speed is generally below 55 m/s. Despite this high threshold, research indicates that the role of turbulence may potentially destabilize the system, leading to a lower flutter instability threshold. This depends on the turbulence characteristics such as intensity and integral lengths when the turbulence is considered in the kinetic pressure as parametric excitations (Barni and Mannini, 2024). In the study, the kinetic pressure is considered to be exclusively contributed by mean wind speeds. Therefore, this parametric effect doesn't play a role and no divergent oscillation is observed.

Additionally, the amplification coefficients for expected extreme responses to non-stationary/non-Gaussian and stationary/Gaussian excitations consistently exceed 1 except some values slightly lower than 1 for rotational responses, possibly due to inadequate built-up time resulting from the given zero initial conditions in non-stationary calculations. In general, the consideration of non-synoptic features of wind speed potentially results in greater extreme responses. Particularly, in specific scenarios, theses coefficients would exceed 1.5, with Segment No. 74 exhibiting an exceptionally excessive coefficient over 2, posing a high risk if these features are disregarded.

6 Conclusion

This study introduces a state augmentation method to investigate the non-stationary/non-Gaussian vibrations of a long-span bridge subjected to non-synoptic wind. This method extends the previously presented approach, applicable to a single degree-of-freedom scenario, to multi-degree-of-freedom scenarios and allows for considerations for unsteady aerodynamic effects. The study incorporates both unsteady motion-induced forces and non-stationary/non-Gaussian turbulence-induced forces to predict the buffeting response. Due to the time-varying mean wind speed, the wind-structure coupled system displays time-dependent characteristics, resulting in non-stationary responses even when wind fluctuations are stationary.

The proposed state augmentation method involves three steps. First, the non-stationary/non-Gaussian excitations are decomposed into stationary/Gaussian counterparts by using the uniformly modulated polynomial model, and the Ornstein–Uhlenbeck processes are employed to represent the derived stationary/Gaussian excitations. Following this, the states of the system and the OU processes are assembled as an augmented form of Itô-type stochastic differential equation. Third, by performing

the defined $\mathcal{M}$ transform of the corresponding Fokker–Planck equation, the statistical moments of the response are determined through solving a first-order ordinary differential equation system. By employing stars and bars method along with symbolic calculations, the moment equations for statistical moments of any order and for dynamic systems with any number of degrees of freedom can be automatically generated.

The proposed method is applied to conduct a comprehensive buffeting analysis of the model bridge concerning all wind segments of Typhoon. In non-stationary cases, as expected, the results indicate considerable variations in RMS responses over time, mirroring the trends observed in time-varying mean wind speed. In scenarios with high turbulence intensity, the incorporation of quadratic terms in buffeting forces has marginal impact on RMS responses but significantly contributes to the non-Gaussian characteristics of the responses. Consequently, this amplifies the peak factor and leads to extreme responses. In summary, the proposed method can adeptly capture the non-stationary/non-Gaussian characteristics of vibrations, showing higher responses when factoring in these non-synoptic features. Notably, the analysis reveals an exceptional case wherein the amplification coefficient for expected extreme responses exceeds 2, signifying substantial risk if these features are disregarded.

Acknowledgements

The study was supported by the National Natural Science Foundation of China (grant No. 51978527, 52008314 and 52278520) and the China Scholarship Council (No.202106260170).

Appendix A

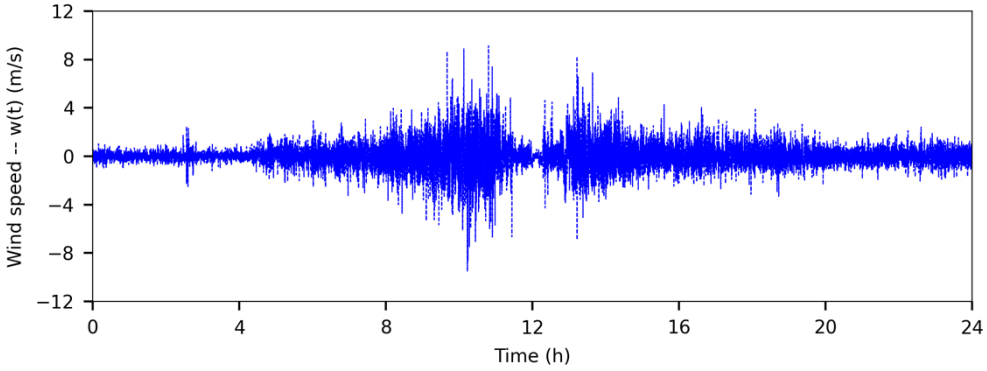

Fig. A.1. Time history of vertical wind speeds of Typhoon Hagupit recorded in September 2008.

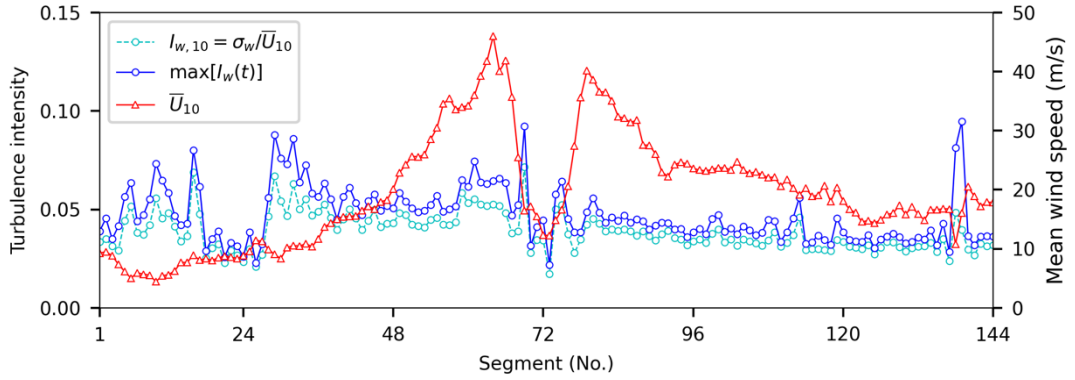

Fig. A.2. Mean wind speeds and vertical turbulence intensities of the subdivided 10-minture segments of Typhoon Hagupit.

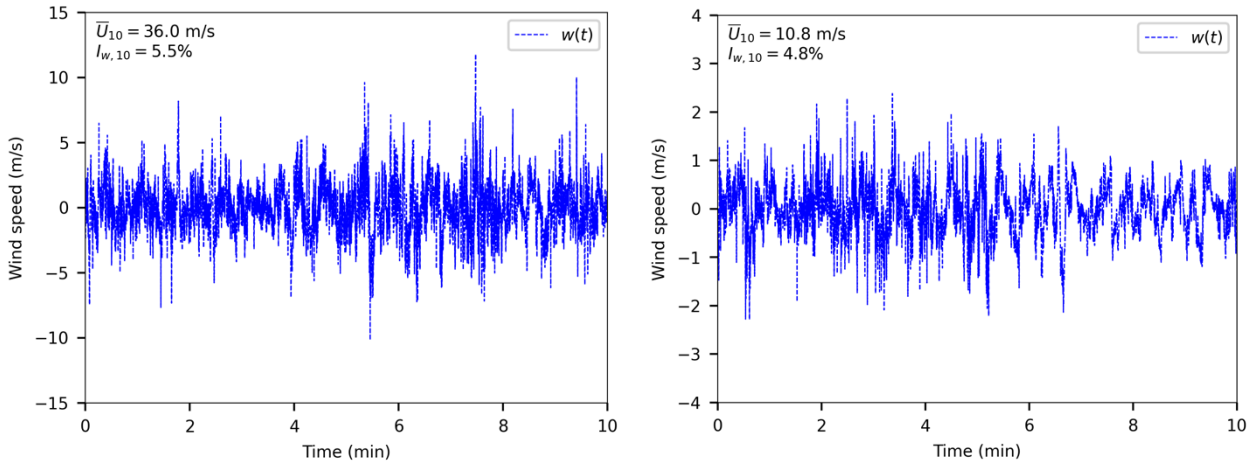

(a) Segment No. 61 (b) Segment No. 138

Fig. A.3. Vertical turbulence of the selected segments from Typhoon Hagupit record.

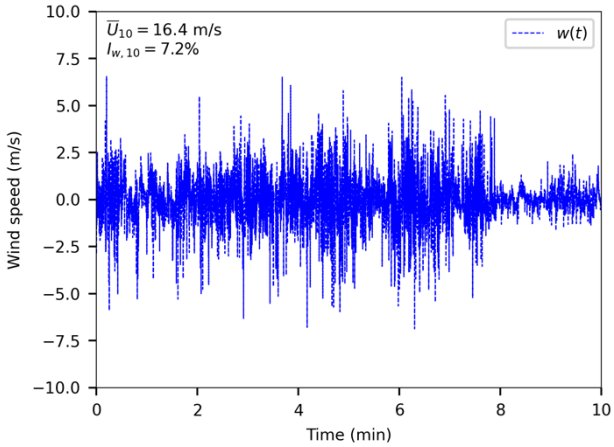

Fig. A.4. Vertical turbulence of Segment No. 69 from Typhoon Hagupit record.

Appendix B

$$\mathbf{Y}(t) = \begin{bmatrix} \mathbf{X} \\ \dot{\mathbf{X}} \\ \mathbf{Z} \end{bmatrix}$$

$$\mathbf{g}(\mathbf{Y}(t),t)=\begin{bmatrix}\mathbf{0} & \mathbf{I} & \mathbf{0}\\ -\mathbf{M}^{-1}\mathbf{K}(t) & -\mathbf{M}^{-1}\mathbf{C}(t) & \mathbf{M}^{-1}\mathbf{A}(t)\\ \mathbf{0} & \mathbf{0} & -\boldsymbol{\alpha}\end{bmatrix}\begin{bmatrix}\mathbf{X}\\ \dot{\mathbf{X}}\\ \mathbf{Z}\end{bmatrix}$$

$$\mathbf{h}(\mathbf{Y}(t),t)=\begin{bmatrix}\mathbf{0}\\ \mathbf{0}\\ \boldsymbol{\Theta}\end{bmatrix}$$

Appendix C

$$\mathcal{M}\left\{\frac{\partial}{\partial t}p(\mathbf{Y},t)\right\}=\int_{-\infty}^{\infty}\cdots\int_{-\infty}^{\infty}\frac{\partial p(\mathbf{Y},t)}{\partial t}\xi(\mathbf{Y})\mathrm{d}Y_1\cdots\mathrm{d}Y_{2N+M}=\frac{\mathrm{d}}{\mathrm{d}t}\mathrm{E}\left[\prod_i^N X_i^{a_i}\prod_i^N \dot{X}_i^{b_i}\prod_i^M Z_i^{f_i}\right]$$

$$\begin{aligned}\mathcal{M}\left\{\frac{\partial g_i p}{\partial Y_i}\right\}&=\int_{-\infty}^{\infty}\cdots\int_{-\infty}^{\infty}\frac{\partial(g_i p)}{\partial Y_i}\xi\mathrm{d}Y_1\cdots\mathrm{d}Y_{2N+M}\\&=\int_{-\infty}^{\infty}\cdots\int_{-\infty}^{\infty}\frac{\partial(g_i p\xi)}{\partial Y_i}\mathrm{d}Y_1\cdots\mathrm{d}Y_{2N+M}-\int_{-\infty}^{\infty}\cdots\int_{-\infty}^{\infty}pg_i\frac{\partial\xi}{\partial Y_i}\mathrm{d}Y_1\cdots\mathrm{d}Y_{2N+M}\\&=\int_{-\infty}^{\infty}\cdots\int_{-\infty}^{\infty}(g_i p\xi)|_{Y_i=-\infty}^{Y_i=\infty}\mathrm{d}Y_1\cdots\mathrm{d}Y_{2N+M}-\mathrm{E}\left[\frac{\partial\xi}{\partial Y_i}g_i\right]=-\mathrm{E}\left[\frac{\partial\xi}{\partial Y_i}g_i\right]\end{aligned}$$

$$\begin{aligned}\mathcal{M}\left\{\frac{\partial^2(\mathbf{h}\mathbf{h}^{\mathrm{T}})_{ij}p}{\partial Y_i\partial Y_j}\right\}&=\int_{-\infty}^{\infty}\cdots\int_{-\infty}^{\infty}\frac{\partial^2(\mathbf{h}\mathbf{h}^{\mathrm{T}})_{ij}p}{\partial Y_i\partial Y_j}\xi\mathrm{d}Y_1\cdots\mathrm{d}Y_{2N+M}\\&=\int_{-\infty}^{\infty}\cdots\int_{-\infty}^{\infty}\frac{\partial}{\partial Y_j}\left(\xi\frac{\partial(\mathbf{h}\mathbf{h}^{\mathrm{T}})_{ij}p}{\partial Y_i}\right)\mathrm{d}Y_1\cdots\mathrm{d}Y_{2N+M}\\&\quad-\int_{-\infty}^{\infty}\cdots\int_{-\infty}^{\infty}\frac{\partial\xi}{\partial Y_j}\frac{\partial(\mathbf{h}\mathbf{h}^{\mathrm{T}})_{ij}p}{\partial Y_i}\mathrm{d}Y_1\cdots\mathrm{d}Y_{2N+M}\\&=\int_{-\infty}^{\infty}\cdots\int_{-\infty}^{\infty}\xi\frac{\partial(\mathbf{h}\mathbf{h}^{\mathrm{T}})_{ij}p}{\partial Y_i}\Bigg|_{Y_j=-\infty}^{Y_j=\infty}\mathrm{d}Y_1\cdots\mathrm{d}Y_{2N+M}\\&\quad-\int_{-\infty}^{\infty}\cdots\int_{-\infty}^{\infty}(\mathbf{h}\mathbf{h}^{\mathrm{T}})_{ij}p\frac{\partial\xi}{\partial Y_j}\Bigg|_{Y_i=-\infty}^{Y_i=\infty}\mathrm{d}Y_1\cdots\mathrm{d}Y_{2N+M}\\&\quad+\int_{-\infty}^{\infty}\cdots\int_{-\infty}^{\infty}(\mathbf{h}\mathbf{h}^{\mathrm{T}})_{ij}p\frac{\partial^2\xi}{\partial Y_i\partial Y_j}\mathrm{d}Y_1\cdots\mathrm{d}Y_{2N+M}\\&=\int_{-\infty}^{\infty}\cdots\int_{-\infty}^{\infty}p(\mathbf{h}\mathbf{h}^{\mathrm{T}})_{ij}\frac{\partial^2\xi}{\partial Y_i\partial Y_j}\mathrm{d}Y_1\cdots\mathrm{d}Y_{2N+M}=\mathrm{E}\left[(\mathbf{h}\mathbf{h}^{\mathrm{T}})_{ij}\frac{\partial^2\xi}{\partial Y_i\partial Y_j}\right]\end{aligned}$$

Appendix D

The following shows an example of how the stars and bars method is implemented to determine

all the combinations of the exponents of statistical moments. Suppose there are 2 stars to be placed into 3 bins, and the bins are allowed to be empty. This is equivalent to the case of 5 stars to be placed into 3 bins with no empty bin allowed, and with one star to be deducted from each bin at the end of the assignment, as is illustrated in Fig. D.1.

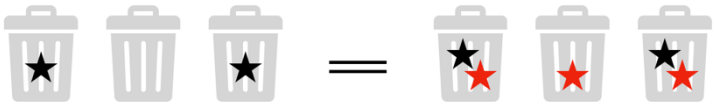

Fig. D.1. Equivalent cases of 2 stars to be placed into 3 bins (empty allowed) and 5 stars to be placed into 3 bins (empty banned) with red stars deducted at the end.

Based on stars and bars method, this can be achieved by placing 2 bars into 4 internal gaps between an alignment of 5 stars and separating the stars into 3 groups, corresponding to 3 bins in sequence. Now number the internal 4 gaps from 1 to 4 in sequence, and also the two sides with 0 and 5, as is shown in Fig. D.2.

Fig. D.2. The ordinal numbers of 4 internal gaps between 5 stars and 2 sides.

Next, all possible combinations of 2 numbers selected from 4 internal gaps with no repeated numbers can be efficiently determined either by Python syntax 'itertools.combinations(iterable, r)' or MATLAB syntax 'combntns(v,k)' as

$$(1\quad 2),\quad (1\quad 3),\quad (1\quad 4),\quad (2\quad 3),\quad (2\quad 4),\quad (3\quad 4),$$

of which the number is $\mathrm{C}_4^2 = 6$. Appending the number 5 to the end of each combination gives

$$(1\quad 2\quad 5),\quad (1\quad 3\quad 5),\quad (1\quad 4\quad 5),\quad (2\quad 3\quad 5),\quad (2\quad 4\quad 5),\quad (3\quad 4\quad 5),$$

and prefixing the number 0 to the front of each combination gives

$$(0\quad 1\quad 2),\quad (0\quad 1\quad 3),\quad (0\quad 1\quad 4),\quad (0\quad 2\quad 3),\quad (0\quad 2\quad 4),\quad (0\quad 3\quad 4).$$

The difference between two expanded combinations is

$$(1\quad 1\quad 3),\quad (1\quad 2\quad 2),\quad (1\quad 3\quad 1),\quad (2\quad 1\quad 2),\quad (2\quad 2\quad 1),\quad (3\quad 1\quad 1),$$

and deducting a value of 1 from each element in each difference combination gives

$$(0\quad 0\quad 2),\quad (0\quad 1\quad 1),\quad (0\quad 2\quad 0),\quad (1\quad 0\quad 1),\quad (1\quad 1\quad 0),\quad (2\quad 0\quad 0).$$

Clearly, this is exactly all possible combinations of 2 stars being placed into 3 bins.

Appendix E

$\mathbf{F}_i^b$ is the vector of non-Gaussian buffeting forces at the i-th node, and can be expressed in a component-wise way as

$$\mathbf{F}_i^b = \mathbf{F}_i^{bu} + \mathbf{F}_i^{bw} + \mathbf{F}_i^{buu} + \mathbf{F}_i^{bww} + \mathbf{F}_i^{buw}$$

$$\mathbf{F}_i^{bu} = \frac{1}{2}\rho B\Delta L U^2 \begin{bmatrix} 2C_D \\ 2C_L \\ 2BC_M \end{bmatrix} \frac{u_i}{U} = \frac{1}{2}\rho B\Delta L U \mathbf{A}_i^u u_i$$

$$\mathbf{F}_i^{bw} = \frac{1}{2}\rho B\Delta L U^2 \begin{bmatrix} C_D' - C_L \\ C_L' + C_D \\ BC_M' \end{bmatrix} \frac{w_i}{U} = \frac{1}{2}\rho B\Delta L U \mathbf{A}_i^w w_i$$

$$\mathbf{F}_i^{buu} = \frac{1}{2}\rho B\Delta L U^2 \begin{bmatrix} C_D \\ C_L \\ BC_M \end{bmatrix} \frac{u_i^2 - \sigma_{u_i}^2}{U^2} = \frac{1}{2}\rho B\Delta L \mathbf{A}_i^{uu}\left(u_i^2 - \sigma_{u_i}^2\right)$$

$$\mathbf{F}_i^{bww} = \frac{1}{2}\rho B\Delta L U^2 \begin{bmatrix} \frac{1}{2}C_D + \frac{1}{2}C_D'' - C_L' \\ \frac{1}{2}C_L + \frac{1}{2}C_L'' + C_D' \\ C_M + \frac{1}{2}C_M'' \end{bmatrix} \frac{w_i^2 - \sigma_{w_i}^2}{U^2} = \frac{1}{2}\rho B\Delta L \mathbf{A}_i^{ww}\left(w_i^2 - \sigma_{w_i}^2\right)$$

$$\mathbf{F}_i^{buw} = \frac{1}{2}\rho B\Delta L U^2 \begin{bmatrix} 2C_D' - 2C_L \\ 2C_L' + 2C_D \\ 2BC_M' \end{bmatrix} \frac{u_i w_i}{U^2} = \frac{1}{2}\rho B\Delta L \mathbf{A}_i^{uw} u_i w_i$$

where $\mathbf{A}_i^u$, $\mathbf{A}_i^w$, $\mathbf{A}_i^{uu}$, $\mathbf{A}_i^{ww}$ and $\mathbf{A}_i^{uw}$ are the corresponding coefficients. In this way, the detailed expressions of the components in Eq. (31) are found to be

$$\mathbf{F}^{bu} = \frac{1}{2}\rho B\Delta L U \mathbf{A}^u \mathbf{u}^s$$

$$\mathbf{F}^{bw} = \frac{1}{2}\rho B\Delta L U \mathbf{A}^w \mathbf{w}^s$$

$$\mathbf{F}^{buu} = \frac{1}{2}\rho B\Delta L \mathbf{A}^{uu}[\mathrm{diag}(\mathbf{u}^s)\mathbf{u}^s - \sigma_u^2 \mathbf{I}_N]$$

$$\mathbf{F}^{bww} = \frac{1}{2}\rho B\Delta L \mathbf{A}^{ww}[\mathrm{diag}(\mathbf{w}^s)\mathbf{w}^s - \sigma_w^2 \mathbf{I}_N]$$

$$\mathbf{F}^{buw} = \frac{1}{2}\rho B\Delta L \mathbf{A}^{uw}\mathrm{diag}(\mathbf{u}^s)\mathbf{w}^s$$

where $\mathbf{A}^u$, $\mathbf{A}^w$, $\mathbf{A}^{uu}$, $\mathbf{A}^{ww}$, and $\mathbf{A}^{uw}$ are the partitioned diagonal matrix of $\mathbf{A}_i^u$, $\mathbf{A}_i^w$, $\mathbf{A}_i^{uu}$, $\mathbf{A}_i^{ww}$ and $\mathbf{A}_i^{uw}$ $(i = 1, \cdots, N)$.

Appendix F

Expressions of $\boldsymbol{\mathcal{A}}(t)$, $\boldsymbol{\mathcal{B}}_u(t)$ and $\boldsymbol{\mathcal{B}}_w(t)$ in Eq. (33).

$\boldsymbol{\mathcal{A}}(t)$

$$
= \begin{bmatrix}
\mathbf{0} & \mathbf{I} & \mathbf{0} & \cdots & \mathbf{0} & \mathbf{0} & \cdots & \mathbf{0} & \mathbf{0} & \cdots & \mathbf{0} \\
-\bar{\mathbf{M}}^{-1}\bar{\mathbf{K}} & -\bar{\mathbf{M}}^{-1}\bar{\mathbf{C}} & \frac{1}{2}\rho U^2 \Delta L \bar{\mathbf{M}}^{-1} & \cdots & \frac{1}{2}\rho U^2 \Delta L \bar{\mathbf{M}}^{-1} & -\frac{U\beta_1 d_1^u}{B}\bar{\mathbf{M}}^{-1} & \cdots & -\frac{U\beta_1 d_{m_u}^u}{B}\bar{\mathbf{M}}^{-1} & -\frac{U\beta_2 d_1^w}{B}\bar{\mathbf{M}}^{-1} & \cdots & -\frac{U\beta_2 d_{m_w}^u}{B}\bar{\mathbf{M}}^{-1} \\
\mathbf{0} & \mathbf{A}_4^{se,q} & -\frac{d_1^{se}U}{B}\mathbf{I} & \cdots & \mathbf{0} & \mathbf{0} & \cdots & \mathbf{0} & \mathbf{0} & \cdots & \mathbf{0} \\
\vdots & \vdots & \vdots & \ddots & \vdots & \vdots & \ddots & \vdots & \vdots & \ddots & \vdots \\
\mathbf{0} & \mathbf{A}_{m_{se}+3}^{se,q} & \mathbf{0} & \cdots & -\frac{d_{m_{se}}^{se}U}{B}\mathbf{I} & \mathbf{0} & \cdots & \mathbf{0} & \mathbf{0} & \cdots & \mathbf{0} \\
\mathbf{0} & \mathbf{0} & \mathbf{0} & \cdots & \mathbf{0} & -\frac{d_1^u U}{B}\mathbf{I} & \cdots & \mathbf{0} & \mathbf{0} & \cdots & \mathbf{0} \\
\vdots & \vdots & \vdots & \ddots & \vdots & \vdots & \ddots & \vdots & \vdots & \ddots & \vdots \\
\mathbf{0} & \mathbf{0} & \mathbf{0} & \cdots & \mathbf{0} & \mathbf{0} & \cdots & -\frac{d_{m_u}^u U}{B}\mathbf{I} & \mathbf{0} & \cdots & \mathbf{0} \\
\mathbf{0} & \mathbf{0} & \mathbf{0} & \cdots & \mathbf{0} & \mathbf{0} & \cdots & \mathbf{0} & -\frac{d_1^w U}{B}\mathbf{I} & \cdots & \mathbf{0} \\
\vdots & \vdots & \vdots & \ddots & \vdots & \vdots & \ddots & \vdots & \vdots & \ddots & \vdots \\
\mathbf{0} & \mathbf{0} & \mathbf{0} & \cdots & \mathbf{0} & \mathbf{0} & \cdots & \mathbf{0} & \mathbf{0} & \cdots & -\frac{d_{m_w}^w U}{B}\mathbf{I}
\end{bmatrix}
$$

in which $\mathbf{A}_l^{se,q} = \boldsymbol{\Psi}^{\mathrm{T}}\mathbf{A}_l^{se}\boldsymbol{\Psi}$ $(l = 1, \cdots, m_{se} + 3)$ are the generalized frequency independent coefficients. $\bar{\mathbf{M}} = \mathbf{M}_q - 0.5\rho B^2 \Delta L \mathbf{A}_3^{se,q}$, $\bar{\mathbf{C}} = \mathbf{C}_q - 0.5\rho U B \Delta L \mathbf{A}_2^{se,q}$, and $\bar{\mathbf{K}} = \mathbf{K}_q - 0.5\rho U^2 \Delta L \mathbf{A}_1^{se,q}$ are on-wind generalized modal mass, damping and stiffness matrices, respectively. $\beta_1 = 0.5\rho U \Delta L \beta^u$ and $\beta_2 = 0.5\rho U \Delta L \beta^w$.

$$\boldsymbol{\mathcal{B}}_u(t) = \begin{bmatrix} \mathbf{0} & \mathbf{0} & \cdots & \mathbf{0} \\ \beta_1\bar{\mathbf{M}}^{-1} & \beta_1\bar{\mathbf{M}}^{-1} & \cdots & \beta_1\bar{\mathbf{M}}^{-1} \\ \mathbf{0} & \mathbf{0} & \cdots & \mathbf{0} \\ \vdots & \vdots & \ddots & \vdots \\ \mathbf{0} & \mathbf{0} & \cdots & \mathbf{0} \\ \mathbf{0} & \mathbf{I} & \cdots & \mathbf{0} \\ \vdots & \vdots & \ddots & \vdots \\ \mathbf{0} & \mathbf{0} & \cdots & \mathbf{I} \\ \mathbf{0} & \mathbf{0} & \cdots & \mathbf{0} \\ \vdots & \vdots & \ddots & \vdots \\ \mathbf{0} & \mathbf{0} & \cdots & \mathbf{0} \end{bmatrix}$$

$$\boldsymbol{\mathcal{B}}_w(t) = \begin{bmatrix} \mathbf{0} & \mathbf{0} & \cdots & \mathbf{0} \\ \beta_2\bar{\mathbf{M}}^{-1} & \beta_2\bar{\mathbf{M}}^{-1} & \cdots & \beta_2\bar{\mathbf{M}}^{-1} \\ \mathbf{0} & \mathbf{0} & \cdots & \mathbf{0} \\ \vdots & \vdots & \ddots & \vdots \\ \mathbf{0} & \mathbf{0} & \cdots & \mathbf{0} \\ \mathbf{0} & \mathbf{I} & \cdots & \mathbf{0} \\ \vdots & \vdots & \ddots & \vdots \\ \mathbf{0} & \mathbf{0} & \cdots & \mathbf{I} \\ \mathbf{0} & \mathbf{0} & \cdots & \mathbf{0} \\ \vdots & \vdots & \ddots & \vdots \\ \mathbf{0} & \mathbf{0} & \cdots & \mathbf{0} \end{bmatrix}$$

Expressions of $\boldsymbol{\mathcal{C}}_{\mathbf{u}}$ and $\boldsymbol{\mathcal{C}}_{\mathbf{w}}$ in Eq. (34) and Eq. (37).

$$\boldsymbol{\mathcal{C}}_{\mathbf{u}} = \begin{bmatrix} \mathcal{C}_u(x_1, x_1, \omega) & \cdots & \mathcal{C}_u(x_1, x_N, \omega) \\ \vdots & \ddots & \vdots \\ \mathcal{C}_u(x_N, x_1, \omega) & \cdots & \mathcal{C}_u(x_N, x_N, \omega) \end{bmatrix}$$

$$\boldsymbol{\mathcal{C}}_{\mathbf{w}} = \begin{bmatrix} \mathcal{C}_w(x_1, x_1, \omega) & \cdots & \mathcal{C}_w(x_1, x_N, \omega) \\ \vdots & \ddots & \vdots \\ \mathcal{C}_w(x_N, x_1, \omega) & \cdots & \mathcal{C}_w(x_N, x_N, \omega) \end{bmatrix}$$

in which

$$\mathcal{C}_u(x_i, x_j, \omega) = \exp\left(-\frac{c_u \omega |x_i - x_j|}{2\pi \max[U]}\right)$$

$$\mathcal{C}_w(x_i, x_j, \omega) = \exp\left(-\frac{c_w \omega |x_i - x_j|}{2\pi \max[U]}\right)$$

Expressions of $\boldsymbol{\mathcal{A}}$ and $\boldsymbol{\mathcal{B}}$ in Eq. (35).

$$\boldsymbol{\mathcal{A}} = \begin{bmatrix} \mathbf{0} & \mathbf{I} & \mathbf{0} & \cdots & \mathbf{0} \\ -\bar{\mathbf{M}}^{-1}\bar{\mathbf{K}} & -\bar{\mathbf{M}}^{-1}\bar{\mathbf{C}} & \frac{1}{2}\rho U^2 \Delta L \bar{\mathbf{M}}^{-1} & \cdots & \frac{1}{2}\rho U^2 \Delta L \bar{\mathbf{M}}^{-1} \\ \mathbf{0} & \mathbf{A}_4^{se,q} & -\frac{d_1^{se} U}{B}\mathbf{I} & \cdots & \mathbf{0} \\ \vdots & \vdots & \vdots & \ddots & \vdots \\ \mathbf{0} & \mathbf{A}_{m_{se}+3}^{se,q} & \mathbf{0} & \cdots & -\frac{d_{m_{se}}^{se} U}{B}\mathbf{I} \end{bmatrix}$$

$$\boldsymbol{\mathcal{B}} = \begin{bmatrix} \mathbf{0} \\ \bar{\mathbf{M}}^{-1} \\ \mathbf{0} \\ \vdots \\ \mathbf{0} \end{bmatrix}$$

Coefficient matrices of Itô-type stochastic differential equation in the case of Eq. (38)

$$\mathbf{g}(\mathbb{Y}(t), t) = \begin{bmatrix} \boldsymbol{\mathcal{A}} & \boldsymbol{\mathcal{B}}_u & \boldsymbol{\mathcal{B}}_w \\ \mathbf{0} & -\boldsymbol{\alpha}^u & \mathbf{0} \\ \mathbf{0} & \mathbf{0} & -\boldsymbol{\alpha}^w \end{bmatrix} \begin{bmatrix} \mathbf{Y} \\ \mathbf{Z}^u \\ \mathbf{Z}^w \end{bmatrix}$$

$$\mathbf{h}(\mathbb{Y}(t), t) = \begin{bmatrix} \mathbf{0} & \mathbf{0} \\ \boldsymbol{\Theta}^u & \mathbf{0} \\ \mathbf{0} & \boldsymbol{\Theta}^w \end{bmatrix}$$

in which $\mathbb{Y} = [\mathbf{Y}^{\mathrm{T}} \quad \mathbf{Z}^{u\mathrm{T}} \quad \mathbf{Z}^{w\mathrm{T}}]^{\mathrm{T}}$.

Coefficient matrices of Itô-type stochastic differential equation in the case of Eq. (39)

$$\mathbf{g}(\mathbb{Y}(t),t)=\begin{bmatrix}\boldsymbol{\mathcal{A}} & \boldsymbol{\mathcal{B}}\sum_{j=1}^{k}\boldsymbol{\Gamma}_j\mathrm{diag}(\mathbf{Z}^{Q})^{j-1}\\ \mathbf{0} & -\boldsymbol{\alpha}^{Q}\end{bmatrix}$$

$$\mathbf{h}(\mathbb{Y}(t),t)=\begin{bmatrix}\mathbf{0}\\ \boldsymbol{\Theta}^{Q}\end{bmatrix}$$

in which $\mathbb{Y}=[\mathbf{Y}^{\mathrm{T}}\quad \mathbf{Z}^{Q\mathrm{T}}]^{\mathrm{T}}$.

References

Barni, N., Mannini, C., 2024. Parametric effects of turbulence on the flutter stability of suspension bridges. Journal of Wind Engineering and Industrial Aerodynamics 245.

Barni, N., Øiseth, O., Mannini, C., 2021. Time-variant self-excited force model based on 2D rational function approximation. Journal of Wind Engineering and Industrial Aerodynamics 211, 104523.

Barni, N., Øiseth, O.A., Mannini, C., 2022. Buffeting response of a suspension bridge based on the 2D rational function approximation model for self-excited forces. Engineering Structures 261, 114267.

Benfratello, S., Falsone, G., Muscolino, G., 1996. Influence of the quadratic term in the alongwind stochastic response of SDOF structures. Engineering Structures 18, 685-695.

Benfratello, S., Muscolino, G., 1999. Filter approach to the stochastic analysis of MDOF wind-excited structures. Probabilistic engineering mechanics 14, 311-321.

Brusco, S., Solari, G., 2021. Transient aeroelasticity of structures subjected to thunderstorm outflows. Engineering Structures 245, 112801.

Chen, X., 2008. Analysis of alongwind tall building response to transient nonstationary winds. Journal of structural engineering 134, 782-791.

Chen, X., 2015. Analysis of multimode coupled buffeting response of long-span bridges to nonstationary winds with force parameters from stationary wind. Journal of Structural Engineering 141, 04014131.

Chen, X., Matsumoto, M., Kareem, A., 2000. Time domain flutter and buffeting response analysis of bridges. Journal of Engineering Mechanics 126, 7-16.

Cui, W., Zhao, L., Ge, Y., 2022. Non-Gaussian turbulence induced buffeting responses of long-span bridges based on state augmentation method. Engineering Structures 254, 113774.

da Costa, B.M., Wang, J.A., Jakobsen, J.B., Oiseth, O.A., Snæbjörnsson, J.P., 2022. Bridge buffeting by skew winds: A revised theory. Journal of Wind Engineering and Industrial Aerodynamics 220.

Davenport, A.G., 1967. Gust loading factors. Journal of the Structural Division 93, 11-34.

Denoël, V., Carassale, L., 2015. Response of an oscillator to a random quadratic velocity-feedback loading. Journal of Wind Engineering and Industrial Aerodynamics 147, 330-344.

Denoël, V., Degée, H., 2006. A simplified method to account for the non linearity of aerodynamic coefficients in the analysis of wind-loaded bridges, NCTAM, 7th National Congres on Theoretical and Applied Mechanics.

Feller, W., 1991. An introduction to probability theory and its applications, Volume 2. John Wiley & Sons.

Fenerci, A., Øiseth, O., 2018. Strong wind characteristics and dynamic response of a long-span suspension bridge during a storm. Journal of Wind Engineering and Industrial Aerodynamics 172, 116-138.

Grigoriu, M., 2013. Stochastic Calculus: Applications in Science and Engineering. Springer Science

& Business Media.

Grigoriu, M., Ariaratnam, S., 1988. Response of linear systems to polynomials of Gaussian processes.

Grigoriu, M., Field Jr, R., 2014. A method for analysis of linear dynamic systems driven by stationary non-Gaussian noise with applications to turbulence-induced random vibration. Applied Mathematical Modelling 38, 336-354.

Gullo, I., Muscolino, G., Vasta, M., 1998. Non-Gaussian probability density function of SDOF linear structures under wind actions. Journal of Wind Engineering and Industrial Aerodynamics 74, 1123-1134.

Guo, Y., Kareem, A., 2016. Non-stationary frequency domain system identification using time–frequency representations. Mechanical Systems and Signal Processing 72, 712-726.

Gurley, K.R., Tognarelli, M.A., Kareem, A., 1997. Analysis and simulation tools for wind engineering. Probabilistic Engineering Mechanics 12, 9-31.

Hu, L., Xu, Y.-L., Huang, W.-F., 2013. Typhoon-induced non-stationary buffeting response of long-span bridges in complex terrain. Engineering Structures 57, 406-415.

Hu, L., Xu, Y.-L., Zhu, Q., Guo, A., Kareem, A., 2017. Tropical storm–induced buffeting response of long-span bridges: Enhanced nonstationary buffeting force model. Journal of Structural Engineering 143, 04017027.

Huang, G., Chen, X., Liao, H., Li, M., 2013. Predicting of tall building response to non-stationary winds using multiple wind speed samples. Wind & structures 17, 227-244.

Huang, G., Zheng, H., Xu, Y.-l., Li, Y., 2015. Spectrum models for nonstationary extreme winds. Journal of Structural Engineering 141, 04015010.

Huang, N.E., Shen, Z., Long, S.R., Wu, M.C., Shih, H.H., Zheng, Q., Yen, N.-C., Tung, C.C., Liu, H.H., 1998. The empirical mode decomposition and the Hilbert spectrum for nonlinear and non-stationary time series analysis. Proceedings of the Royal Society of London. Series A: mathematical, physical and engineering sciences 454, 903-995.

Isyumov, N., 2012. Alan G. Davenport's mark on wind engineering. Journal of Wind Engineering and Industrial Aerodynamics 104, 12-24.

Itô, K., 1944. 109. stochastic integral. Proceedings of the Imperial Academy 20, 519-524.

Jain, A., Jones, N.P., Scanlan, R.H., 1996. Coupled flutter and buffeting analysis of long-span bridges. Journal of Structural Engineering 122, 716-725.

Jones, N.P., Scanlan, R.H., 2001. Theory and full-bridge modeling of wind response of cable-supported bridges. Journal of Bridge Engineering 6, 365-375.

Kareem, A., 2009. The changing dynamics of aerodynamics: New frontiers, Proceedings of the 7th Asia-Pacific Conference on Wind Engineering (APCWQ-VII), Taiwan, China, pp. 8-12.

Kareem, A., Hu, L., Guo, Y., Kwon, D.-K., 2019. Generalized wind loading chain: Time-frequency modeling framework for nonstationary wind effects on structures. Journal of Structural Engineering 145, 04019092.

Kareem, A.a., Tognarelli, M., Gurley, K., 1998. Modeling and analysis of quadratic term in the wind effects on structures. Journal of Wind Engineering and Industrial Aerodynamics 74, 1101-1110.

Karlin, S., Taylor, H.E., 1981. A second course in stochastic processes. Elsevier.

Lei, S., Cui, W., Patruno, L., de Miranda, S., Zhao, L., Ge, Y., 2022a. Improved state augmentation method for buffeting analysis of structures subjected to non-stationary wind. Probabilistic Engineering Mechanics 69, 103309.

Lei, S., Ge, Y., Li, Q., Thompson, D.J., 2022b. Wave interference in railway track due to multiple wheels. Journal of Sound and Vibration 520, 116620.

Lin, J., Zhang, W., Williams, F., 1994. Pseudo-excitation algorithm for nonstationary random seismic responses. Engineering Structures 16, 270-276.

Lin, Z., Qi, W., Shenyou, S., Weile, C., Mingyuan, W., Haili, L., Yaojun, G., 2019. Investigation of Wind-resistance Performance of Lingdingyang Bridge with Main-span 1666 m in Shen-Zhong Link. China Journal of Highway and Transport 32, 57-66.

Liu, P., Zhao, L., Fang, G.S., Ge, Y.J., 2021. Explicit polynomial regression models of wind characteristics and structural effects on a long-span bridge utilizing onsite monitoring data. Structural Control & Health Monitoring 28.

Lombaert, G., Conte, J.P., 2012. Random vibration analysis of dynamic vehicle-bridge interaction due to road unevenness. Journal of Engineering Mechanics 138, 816-825.

Lu, F., Lin, J., Kennedy, D., Williams, F.W., 2009. An algorithm to study non-stationary random vibrations of vehicle–bridge systems. Computers & Structures 87, 177-185.

Lyapunov, A.M., 1892. The general problem of motion stability. Annals of Mathematics Studies 17.

Meurer, A., Smith, C.P., Paprocki, M., Čertík, O., Kirpichev, S.B., Rocklin, M., Kumar, A., Ivanov, S., Moore, J.K., Singh, S., 2017. SymPy: symbolic computing in Python. PeerJ Computer Science 3, e103.

Page, C.H., 1952. Instantaneous power spectra. Journal of Applied Physics 23, 103-106.

Priestley, M., 1967. Power spectral analysis of non-stationary random processes. Journal of Sound and Vibration 6, 86-97.

Priestley, M.B., 1965. Evolutionary spectra and non ‐ stationary processes. Journal of the Royal Statistical Society: Series B (Methodological) 27, 204-229.

Scanlan, R.H., 1993. Problematics in formulation of wind-force models for bridge decks. Journal of engineering mechanics 119, 1353-1375.

Soong, T.T., Grigoriu, M., 1993. Random vibration of mechanical and structural systems. NASA STI/Recon Technical Report A 93, 14690.

Sun, J.-Q., Hsu, C., 1987. Cumulant-neglect closure method for nonlinear systems under random excitations.

Tao, T., Xu, Y.-L., Huang, Z., Zhan, S., Wang, H., 2020. Buffeting analysis of long-span bridges under typhoon winds with time-varying spectra and coherences. Journal of Structural Engineering 146,

04020255.

Wickerhauser, M., 1992. 2] RR Coifman, Y. Meyer, and MV Wickerhauser, Wavelet analysis and signal pro-cessing, Wavelets and Their Applications, ed. Ruskai et al., ISBN 0-86720-225-4, Jones and Bartlett, Boston, 1992, pp. 153 178. IEEE Transactions on Information Theory 32, 712-718.

Wojtkiewicz, S., Spencer Jr, B., Bergman, L., 1996. On the cumulant-neglect closure method in stochastic dynamics. International journal of non-linear mechanics 31, 657-684.

Xu, S.Y., Fang, G.S., Zhao, L., Ge, Y.J., Zhang, J.F., 2023. Aerodynamic and Aerostatic Performance of a Long-Span Bridge with Wide Single Box Girder Installed with Vertical and Horizontal Stabilizers. Journal of Structural Engineering 149.

Zadeh, L.A., 1950. The determination of the impulsive response of variable networks. Journal of Applied Physics 21, 642-645.

Zhang, L., Cui, W., Zhao, L., Ge, Y., 2023. State augmentation method for buffeting responses of wind-sensitive structures in wind environments with large turbulence intensity. Journal of Wind Engineering and Industrial Aerodynamics 240, 105498.

Zhang, Z., Lin, J., Zhang, Y., Zhao, Y., Howson, W.P., Williams, F.W., 2010. Non-stationary random vibration analysis for train–bridge systems subjected to horizontal earthquakes. Engineering Structures 32, 3571-3582.

Zhao, L., Cui, W., Ge, Y., 2019. Measurement, modeling and simulation of wind turbulence in typhoon outer region. Journal of Wind Engineering and Industrial Aerodynamics 195, 104021.